Article

Immune-evasive human islet-like organoids ameliorate diabetes

https://doi.org/10.1038/s41586-020-2631-z

Received: 17 December 2018

Accepted: 18 May 2020

Published online: 19 August 2020

Check for updates

Eiji Yoshihara[1,5,6], Carolyn O'Connor[2], Emanuel Gasser[1], Zong Wei[1,7], Tae Gyu Oh[1], Tiffany W. Tseng[1], Dan Wang[1], Fritz Cayabyab[1], Yang Dai[1], Ruth T. Yu[1], Christopher Liddle[3], Annette R. Atkins[1], Michael Downes[1] & Ronald M. Evans[1,4] ✉

Islets derived from stem cells hold promise as a therapy for insulin-dependent diabetes, but there remain challenges towards achieving this goal[1–6]. Here we generate human islet-like organoids (HILOs) from induced pluripotent stem cells and show that non-canonical WNT4 signalling drives the metabolic maturation necessary for robust ex vivo glucose-stimulated insulin secretion. These functionally mature HILOs contain endocrine-like cell types that, upon transplantation, rapidly re-establish glucose homeostasis in diabetic NOD/SCID mice. Overexpression of the immune checkpoint protein programmed death-ligand 1 (PD-L1) protected HILO xenografts such that they were able to restore glucose homeostasis in immune-competent diabetic mice for 50 days. Furthermore, ex vivo stimulation with interferon-γ induced endogenous PD-L1 expression and restricted T cell activation and graft rejection. The generation of glucose-responsive islet-like organoids that are able to avoid immune detection provides a promising alternative to cadaveric and device-dependent therapies in the treatment of diabetes.

Islet transplantation provides superior long-term blood glucose control for people with type 1 and late-stage type 2 diabetes; however, the availability and quality of cadaveric islets limits its success and utility. Although the differentiation of induced pluripotent stem cells (iPS cells) into insulin-producing β-like cells represents a major advance, the science needed to generate functional β-like cells appropriate for human therapy remains incomplete[1–6]. Towards this end, we previously demonstrated that the nuclear oestrogen-related receptor γ (ERRγ) drives a postnatal metabolic maturation program necessary for β-cell glucose-stimulated insulin secretion (GSIS)[1]. Furthermore, ERRγ overexpression in β-like cells derived from iPS cells is sufficient for in vitro and in vivo functionality[1]. With the goal of generating functional cells suitable for transplantation, we explored culture conditions designed to replicate the cellular architecture, as well as the cell-type diversity of islets. We initially exploited the cell-intrinsic abilities of human adipose-derived stem cells (hADSCs) and human umbilical vein endothelial cells (HUVECs)—which mimic pancreatic fibroblast and pancreatic endothelial cells, respectively—to form organ-like and vascular structures when grown in three-dimensional (3D) cultures (Extended Data Fig. 1a–c and data not shown), and a polysaccharide-based suspension gel (gellan gum). Incorporating hADSCs and HUVECs during the differentiation of human iPS cell (hiPS cell)-derived endocrine progenitors in a 3D gellan gum gel led to the formation of multicellular spheroids (MCSs) comparable in size to human islets (Extended Data Fig. 1d). The MCSs contained insulin-producing cells and incorporated hADSCs, indicated by the presence of cells containing lipid droplets (Extended Data Fig. 1d). Furthermore, the increased expression of *ESRRG* (which encodes ERRγ) and the mitochondrial genes *NDUFA1* and *COX7A2* in MCSs compared with differentiation in the absence of hADSCs and HUVECs, correlated with improved in vitro insulin secretion in response to a glucose challenge (Extended Data Fig. 1e, f). MCSs transplanted into the kidney capsule were able to maintain glucose homeostasis for about 40 days in streptozotocin (STZ)-induced diabetic NOD/SCID mice, displaying similar efficacy to human islet transplantations (Extended Data Fig. 1g). Moreover, transplanted MCSs remained glucose responsive, appropriately regulating insulin secretion in the fed, fasted and refed states, as indicated by levels of human C-peptide (Extended Data Fig. 1h; mouse insulin levels were less than 0.2 ng ml^{-1}, data not shown). These results support the role of 3D multicellular interactions in organogenesis[7,8].

Gene ontology of the transcriptional changes induced during hADSC self-assembly identified enrichment of metabolic and cytokine signalling pathways, as well as WNT signalling (Extended Data Fig. 1i, Supplementary Table 1). Consistent with this, the temporal expression of WNT genes during hADSC self-assembly revealed a transient, approximately twofold increase in *WNT5A* expression that coincided with the initial cell–cell interactions observed in 3D cultures (Extended Data Fig. 1j). *WNT4* expression is enhanced during the postnatal functional maturation of mouse islets, and the non-canonical WNT pathway has been shown to induce β-cell maturation and increase GSIS in human islets[1,9]. In agreement with these findings, *WNT4* was highly expressed in human islets (Extended Data Fig. 2a). Moreover, single-cell sequencing of human islets identified widespread expression of *WNT4* in β and α cells, along with more restricted *WNT5A* expression predominantly in stellate cells (Extended Data Fig. 2b–f). On the basis of these findings, we proposed that WNT signalling was sufficient for ex vivo functional

[1]Gene Expression Laboratory, Salk Institute for Biological Studies, La Jolla, CA, USA. [2]Flow Cytometry Core Facility, Salk Institute for Biological Studies, La Jolla, CA, USA. [3]Storr Liver Centre, Westmead Institute for Medical Research and Sydney Medical School, University of Sydney, Westmead, New South Wales, Australia. [4]Howard Hughes Medical Institute, Salk Institute for Biological Studies, La Jolla, CA, USA. [5]The Lundquist Institute for Biomedical Innovation, Harbor–UCLA Medical Center, Torrance, CA, USA. [6]David Geffen School of Medicine at UCLA, Los Angeles, USA. [7]Present address: Department of Physiology and Biomedical Engineering, Mayo Clinic, Scottsdale, AZ, USA. ✉e-mail: evans@salk.edu

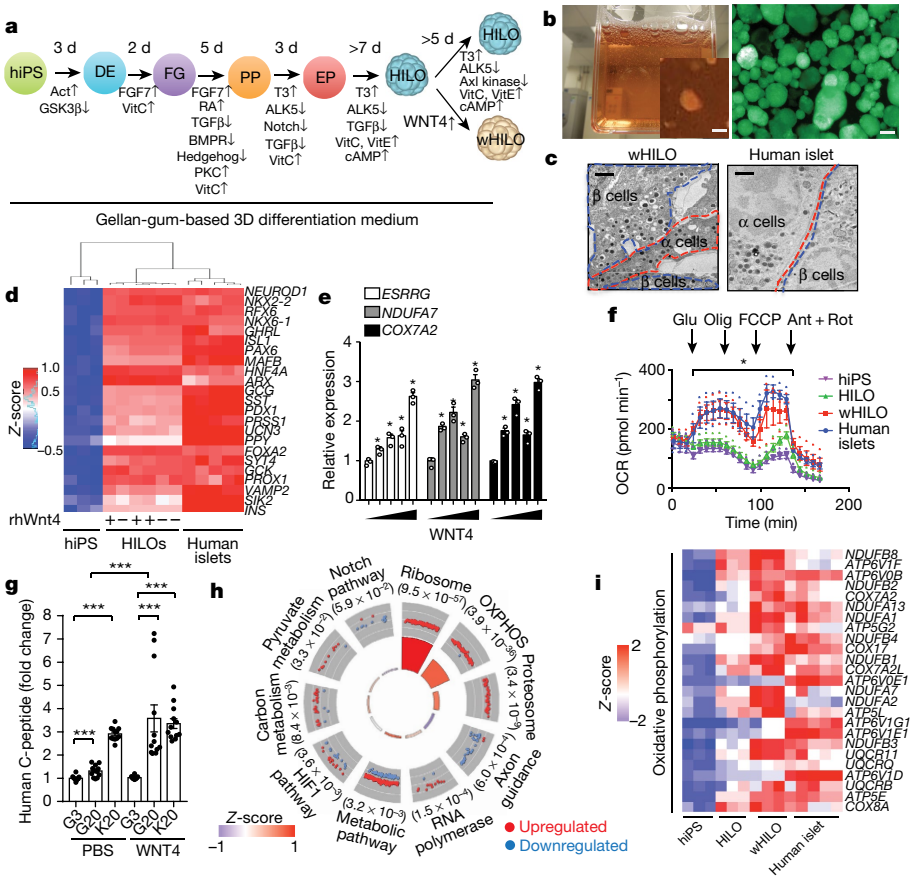

Fig. 1 | WNT4 induces functional maturation of HILOs. a, Schematic showing generation of HILOs. Key factors added to the medium for each developmental step are indicated, with up and down arrows indicating agonists and inhibitors, respectively. DE, definitive endoderm; EP, endocrine progenitors; FG, posterior foregut; PP, pancreatic progenitor. Act, activin A; RA, retinoic acid; VitC, vitamin C; VitE, vitamin E. ALK5 is also known as TGFBR1. **b**, Representative images of HILOs in 3D culture (left) and insulin expression as indicated by GFP expression driven by the human insulin promoter (right). Scale bars, 100 µm. **c**, Electron microscopy images of wHILOs and human islets showing insulin and glucagon granules. Scale bars, 1 µm. **d**, Heat map of relative expressions of key islet genes in hiPS cells ($n = 3$), HILOs treated with PBS (−) ($n = 3$) or recombinant human WNT4 (rhWNT4) (+) ($n = 3$), and human islets ($n = 5$) ($\log_2$ expression with Z-score). **e**, Relative expression of *ESRRG*, *NDUFA7* and *COX7A2* in HILOs after treatment with increasing concentrations of WNT4 (0, 10, 25, 50 or 200 ng ml^{-1} for 5 days, indicated by wedge) ($n = 3$). **f**, Oxygen consumption rate (OCR) measured in hiPS cell spheroids (day 0, purple), PBS-treated HILOs (green), WNT4-treated HILOs (red) and human islets (blue) ($n = 3$). Ant, antimycin A; Glu, glucose; Olig, oligomycin; Rot, rotenone. **g**, In vitro human C-peptide secretion in response to 3 mM (G3) or 20 mM (G20) glucose or 20 mM KCl (K20) from HILOs generated with or without WNT4 treatment. $n = 12$. Fold change relative to G3 PBS. **h**, Gene ontology of WNT4-regulated genes in HILOs (100 ng ml^{-1} WNT4 from day 26 to day 33). Upregulated and downregulated genes in enriched pathways (P values shown in parentheses) are shown in red and blue dots, respectively. Z-scores shown in central wedges. **i**, Heat map of relative expression of oxidative phosphorylation genes in 3D cultured hiPS cells ($n = 3$), HILOs ($n = 3$), wHILOs ($n = 3$) and human islets ($n = 5$) (Z-score). Data are mean ± s.e.m. *$P < 0.05$, ***$P < 0.001$; one-tailed, paired Student's t-test. Data are representative of three independent experiments (**c**, **e**–**g**).

maturation of iPS cell-derived β-like cells. To explore this notion, we used CRISPR–Cas9 genome editing to insert the GFP-coding sequence downstream of the *INS* promoter in hiPS cells (Extended Data Fig. 3a), to generate a reporter for endogenous insulin promoter activity. Differentiation of these engineered hiPS cells in a fully chemically defined 3D-culture system that incorporated WNT4 in a final maturation step led to the formation of human islet-like organoids (HILOs) that express insulin (Fig. 1a, b). In addition, high expression of urocortin-3 (UCN3, secreted from β-cells to regulate δ-cell somatostatin secretion[10–12]) and insulin was observed in HILOs, as visualized with a double-reporter line (*INS* promoter-driven GFP and *UCN3* promoter-driven red fluorescent protein (RFP), Extended Data Fig. 3b). Moreover, analysis of HILOs by electron microscopy revealed structural similarities to human islets, most notably the presence of insulin and glucagon granules (Fig. 1c).

Comparative transcriptional analyses confirmed similar expression of multiple key islet cell markers in WNT4-treated HILOs (wHILOs) and human islets, including β-cell-specific (*NKX6-1*, *NEUROD1*, *RFX6*, *GCK*, *ISL1*, *SYT4* and *PDX1*) and α-cell-specific (*ARX*) genes, whereas *INS*, *MAFA*, *MAFB*, *UCN3* and *NKX2-2* exhibited lower expression (Fig. 1d, Extended Data Fig. 3c). Of note, the expression of β-cell lineage-specification markers including *INS*, *NKX6-1*, *UCN3*, *MAFB* and *SYT4* was not altered by the addition of WNT4, indicating that WNT signalling was not affecting cell fate determination. By contrast, WNT4 dose-dependently increased the expression of *ESRRG* as well as components of the mitochondrial respiratory chain *NDUFA7* and *COX7A2* in HILOs (Fig. 1e). Consistent with these changes in gene expression, HILOs generated in the presence of WNT4 displayed increased oxidative metabolism, as measured by an increase in oxygen consumption rate and decreased extracellular acidification rate, replicating the metabolic characteristics of healthy human islets[13] (Fig. 1f, Extended Data Fig. 3d). WNT4-treated HILOs showed improved in vitro GSIS, an effect that was not blocked by the β-catenin inhibitor XAV939, implicating non-canonical WNT signalling as the driver of WNT4-induced β-cell maturation[14] (Fig. 1g, Extended Data Fig. 3e, f). Similar transcriptional and functional changes were observed during the differentiation and maturation of pluripotent HuES8 and H1ES cells, demonstrating the robustness of our protocol (Extended

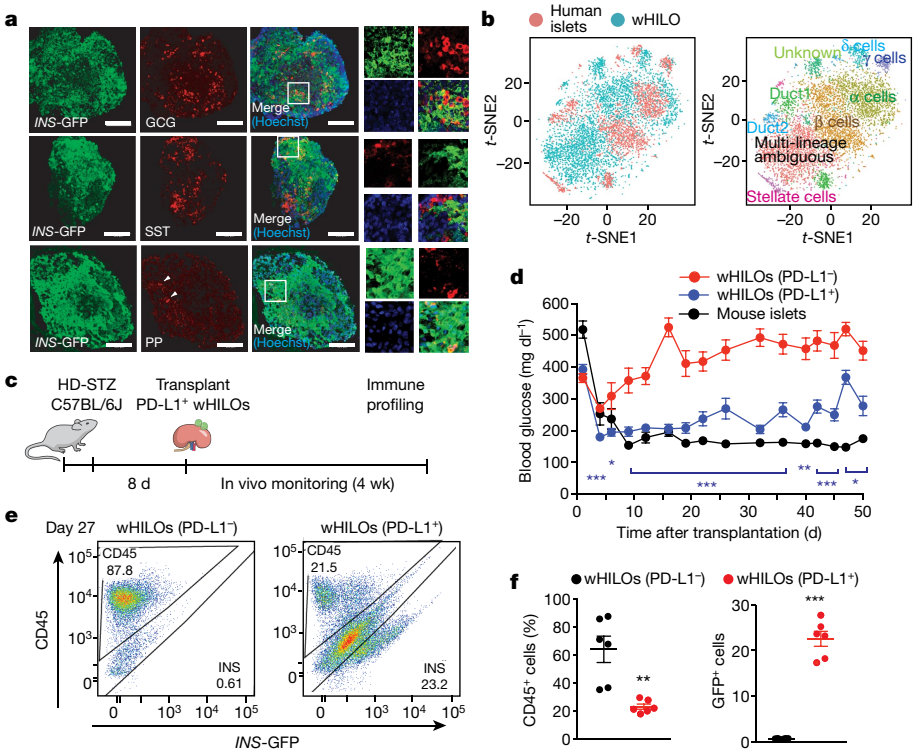

Fig. 2 | Exogenous PD-L1 expression extends wHILO functionality in immune-competent mice. a, Representative immunofluorescence staining for glucagon (GCG; α cell marker), somatostatin (SST; δ cell marker) and pancreatic polypeptide (PP; γ cell marker) in wHILOs. β cells are indicated by GFP expression from the *INS* promoter. Scale bars, 75 µm. Right, expansions of boxed regions. **b**, *t*-Distributed stochastic neighbour embedding (*t*-SNE) clustering of combined wHILO (blue dots, $n = 4{,}840$) and human islet (red dots, $n = 3{,}245$) single-cell transcriptomes (left) and cell types defined by this clustering analysis (left). **c**, Schematic of experimental protocol. High-dose STZ (HD-STZ, 180 mg kg^{-1})-induced diabetic C57BL6J mice received transplants of wHILOs with or without PD-L1 overexpression ($n = 500$) or mouse islets. **d**, Random-fed blood glucose levels after transplantation of wHILOs with or without PD-L1 expression ($n = 11$ and 9, respectively), and C57BL6J islets ($n = 7$). **e**, Flow cytometric analysis of insulin-expressing and mouse immune (CD45$^+$) cells recovered from kidney capsule grafts 27 days after transplantation of wHILOs with or without PD-L1 expression ($n = 6$). Percentage of cells in each region is indicated. **f**, Quantification of analyses in **d**. Data are mean ± s.e.m. $^*P < 0.05$, $^{**}P < 0.01$, $^{***}P < 0.001$; one-tailed, paired Student's *t*-test. Images are representative of three independent experiments. Data are representative (**e**), or compiled from three independent samples (**b**) or experiments (**d**, **f**).

Data Fig. 3g, h). Furthermore, culturing commercially available hiPS cell-derived β-like cells in 3D-differentiation medium containing WNT4 promoted pseudoislet formation and GSIS functionality (Extended Data Fig. 3i, j). Notably, transplanted wHILOs restored glycaemic control in STZ-induced NOD/SCID diabetic mice and maintained glucose homeostasis for more than six weeks (Extended Data Fig. 3k). Together, these results indicate that non-canonical WNT signalling is sufficient to induce the metabolic maturation of HILOs needed for robust GSIS.

To understand the molecular transformations driving the maturation of HILOs, we identified the transcriptional changes induced by WNT4 treatment. The expression of 1,581 genes was increased and that of 1,354 genes was decreased by WNT4 treatment (100 ng ml^{-1} for days 26–33). Gene ontology identified metabolic pathways, most notably oxidative phosphorylation, enriched in the upregulated gene set (Fig. 1h, genes associated with the ribosome include mitochondrial translation and elongation gene clusters as determined by DAVID GOTERM_BP analysis, Extended Data Fig. 3l). Consistent with an effect on cellular metabolism, WNT4 treatment comprehensively increased the expression of OxPhos genes in HILOs to levels similar to those seen in human islets, and increased mitochondrial content (Fig. 1i, Extended Data Fig. 4a). To examine the specific effects on the β-like cell population, insulin-expressing cells were sorted on the basis of GFP expression from HILOs with and without WNT4 or WNT5a treatment. The proportion of insulin-expressing cells was not affected by WNT treatment, in agreement with the invariant β-cell lineage marker expression during HILO maturation (Extended Data Fig. 4b). However, WNT4 and WNT5a treatment increased the mitochondria mass in the insulin-expressing cells, supporting the notion that mitochondrial content underpins the metabolic maturation of β-like cells (Extended Data Fig. 4b). To identify genetic effectors of this maturation step, WNT4-induced changes in chromatin accessibility were mapped in sorted GFP$^+$ cells using assay for transposase-accessible chromatin using sequencing (ATAC–seq). Widespread minor alterations in chromatin accessibility were seen with WNT4 treatment. Gene ontology of the 123 genes with increases in expression and chromatin accessibility upon WNT4 treatment identified metabolic pathways, including oxidative phosphorylation, whereas motif analysis of this gene subset identified β-cell maturation factors including FOXA2 and ERRs (Extended Data Fig. 4c, d). Moreover, WNT4-induced increases in chromatin accessibility were seen at oxidative phosphorylation genes, including the ERRγ-target genes *NDUFA4*, *NDUFA7* and *ATP5E* (Extended Data Fig. 4e). Furthermore, WNT4 (100 ng ml^{-1} for 5 days) induced the expression of mitochondrial metabolic genes and improved GSIS function in isolated neonatal islets from wild-type but not ERRγ β-cell specific knockout mice (ERRγKO mice; Extended Data Fig. 5a, b). Together, these results support the notion that non-canonical WNT4 signalling enhances mitochondrial function, in large part through the induction of an ERRγ gene network that drives the metabolic maturation of β-like cells.

Cellular complexity of mature HILOs

Immunohistochemical and flow cytometric analyses revealed that around 50–60% of wHILO cells coexpressed insulin and β-cell markers, and identified minor cell populations that express markers of other

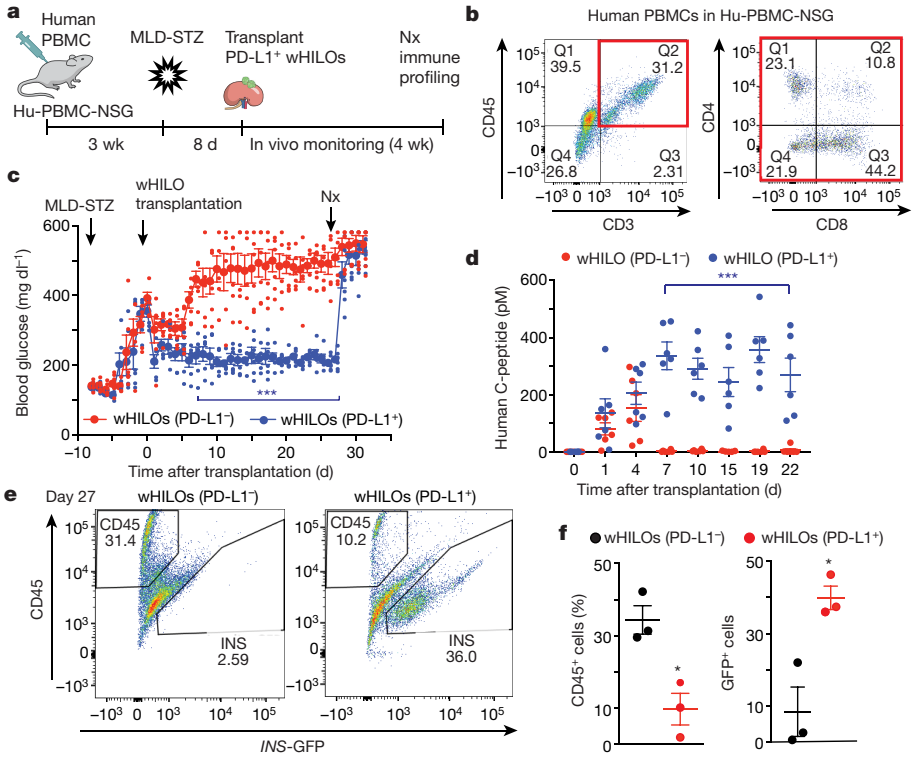

Fig. 3 | wHILOs (PD-L1) provide extended glucose control in humanized mice. a, Schematic showing transplantation of wHILOs with and without PD-L1 overexpression (500 HILOs per mouse) into multiple low-dose STZ (MLD-STZ, 50 mg kg^{-1} day^{-1} for 5 days)-induced diabetic humanized mice (human peripheral blood mononuclear cell (PBMC)-engrafted NSG mice; Hu-PBMC-NSG). Nx, nephrectomy. **b**, Flow cytometric analysis of human T cells (CD4$^+$ and CD8$^+$ cells in the CD45$^+$CD3$^+$ population) in peripheral blood mononuclear cells (PBMCs) from Hu-PBMC-NSG mice ($n = 15$ mice), 3 weeks after human PBMC transplantation. Percentage of cells in each quadrant is shown. **c**, Random-fed blood glucose levels in MLD-STZ-induced diabetic Hu-PBMC-NSG mice after transplantation of wHILOs with or without PD-L1 expression ($n = 6$). **d**, Serum human C-peptide levels in mice described in **c** ($n = 6$). **e**, Flow cytometric analysis of insulin-expressing and human CD45$^+$ immune cells recovered from kidney capsule grafts 27 days after transplantation of wHILOs with and without PD-L1 expression. **f**, Quantification of analyses in **e** ($n = 3$). Data are mean ± s.e.m. *$P < 0.05$, **$P < 0.01$, ***$P < 0.001$; one-tailed, paired Student's t-test. Data are representative (**b**, **e**) or compiled from (**c**, **d**, **f**) two independent experiments.

endocrine cells (glucagon$^+$, somatostatin$^+$, pancreatic polypeptide$^+$) (Fig. 2a, Extended Data Figs. 6a–e, 7a, b). In agreement with the transcriptional comparisons, the cellular composition of HILOs was not altered by WNT4 treatment (Extended Data Fig. 7b). To characterize the cellular complexity of metabolically mature HILOs and gain insight into the in vitro maturation program, we compared the single-cell transcriptomes of HILOs (PBS treated, $n = 4{,}078$) and wHILOs (WNT4 treated, $n = 4{,}840$), with those of human islets ($n = 3{,}245$) (Supplementary Table 2). Clustering of wHILOs revealed populations enriched in β-cell markers, as well as *SOX9*$^+$*HES1*$^+$ pancreatic progenitor clusters (Extended Data Fig. 8a–d). Signature gene expression analyses further distinguished non-replicating and replicating ductal-endocrine bipotent cells (TOP2A$^{\pm}$), hormone-positive endocrine-enriched cells (GCG$^+$ or SST$^+$), ductal-like cells (KRT19$^+$), and a small population of cells with unknown function (Extended Data Fig. 8e, f). Clustering of the integrated HILO and wHILO single-cell RNA sequencing (scRNA-seq) datasets revealed largely similar expression of the lineage markers *INS*, *NEUROD1*, *NKX6-1* and *PDX-1* in the β-like cell cluster (Extended Data Fig. 8g). By contrast, expression of *ESRRG* and its target mitochondrial gene *NDUFV3* were increased and the glycolytic gene *LDHA* was decreased, by WNT4 treatment in *INS*$^+$*ESRRG*$^+$ cells (Extended Data Fig. 8h, i). A similar integrated analysis of wHILO and human islet single-cell datasets confirmed the presence of multiple endocrine-like cell types (Fig. 2b). Although differences were evident (Supplementary Table 3), wHILO cells clustered with islet endocrine cells including β-, α-, δ- and γ-cells, indicating transcriptional similarities (Fig. 2b). Notably, a functional classification based on co-clustering with islet cell types revealed a predominance of β-like and α-like cells in wHILOs (Fig. 2b).

PD-L1 provides immune protection for HILOs

The clinical utility of transplanted islets is limited by both allogenic and autoimmune responses. Of note, subsets of cells in healthy islets including a small number of β-cells were found to express PD-L1 (Extended Data Fig. 9a, b), a known determinant of immune tolerance in β-cells[15–21], leading to the hypothesis that exogenous PD-L1 expression would protect wHILOs from immune rejection. To investigate this notion, PD-L1-expressing hiPS cell clones were generated using a lentiviral system and subsequently differentiated into metabolically mature wHILOs as described in Fig. 1a; PD-L1 overexpression did not affect insulin expression (Extended Data Fig. 9c, d). Transplantation of wHILOs with and without PD-L1 expression into immune-competent diabetic mice restored glycaemic control within days of transplantation with similar efficacy (STZ-treated C57BL6J mice; Fig. 2c, d, Extended Data Fig. 9e). However, the functionality of wHILOs lacking PD-L1 was progressively lost, as indicated by the increases in blood glucose levels, whereas PD-L1$^+$ wHILOs maintained glucose homeostasis for more than 50 days (Fig. 2d). Furthermore, increasing the number of PD-L1$^+$ wHILOs (transplantation of 1,000 wHILOs) normalized blood glucose levels for more than 50 days (Extended Data Fig. 9f). Flow cytometry analyses of grafts recovered 27 days after transplantation revealed decreased numbers of CD45$^+$ immune cells including T cells and natural killer cells in PD-L1$^+$ grafts, as well as negligible numbers of insulin-expressing cells in PD-L1$^-$ grafts (Fig. 2e, f, Extended Data Fig. 10a–c).

The persistence of PD-L1$^+$ wHILOs as xenografts led us to explore their functionality in a model incorporating a reconstituted human T cell repertoire. After confirming the presence of human T cells,

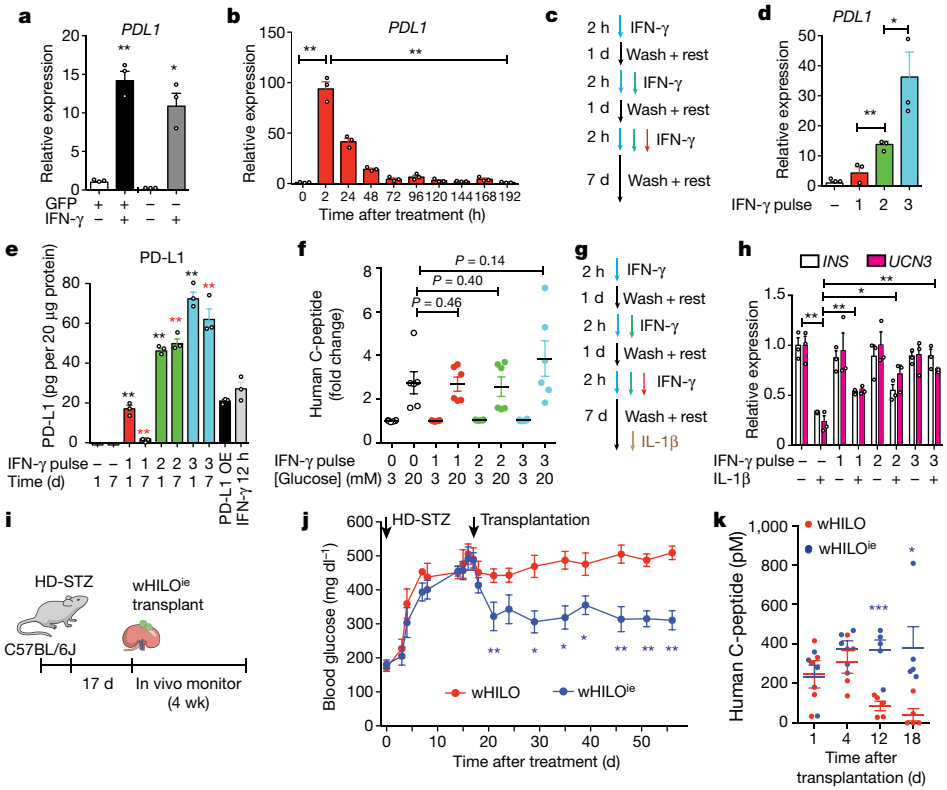

Fig. 4 | Enhanced endogenous PD-L1 expression generates immune-evasive wHILOs. a, *PDL1* expression in cells sorted for expression from the insulin promoter (GFP$^+$ and GFP$^-$, respectively) in wHILOs after IFN-γ treatment (10 ng ml^{-1}, 12 h). **b**, Temporal *PDL1* expression in wHILOs after a single IFN-γ treatment (10 ng ml^{-1}, 2 h). **c**, **d**, Schematic of IFN-γ (10 ng ml^{-1})-pulse treatment (**c**). **d**, *PDL1* expression induced by indicated cycles of IFN-γ treatment, 7 days after last treatment. **e**, PD-L1 protein levels 1 and 7 days after indicated IFN-γ (10 ng ml^{-1}) treatments. PD-L1-overexpressing wHILOs (PDL1 OE) and a single 12 h exposure to IFN-γ were used as positive control. **f**, Human C-peptide secretion from IFN-γ-treated wHILOs in response to 3 mM (G3) or 20 mM (G20) glucose. **g**, Schematic of IFN-γ treatment in combination with an IL-1β challenge (10 ng ml^{-1} for 24 h) to induce β-cell dedifferentiation. **h**, *INS* and *UCN3* expression after indicated IFN-γ and IL-1β treatments of wHILOs. **i**, Schematic of experimental protocol. High-dose STZ (HD-STZ, 180 mg kg^{-1})-induced diabetic C57BL6J mice received transplants of 500 wHILOs with or without the IFN-γ treatment shown in **c**. **j**, Blood glucose levels in recipient mice after transplantation at day 17 of wHILOs or IFN-γ multiple-pulse-stimulated wHILO (wHILO^{ie}) ($n = 6$). **k**, Serum human C-peptide levels in mice described in **i** ($n = 5$). Data are mean ± s.e.m. *$P < 0.05$, **$P < 0.01$; one-tailed, paired Student's *t*-test. $n = 3$ (**a**, **b**, **d**, **e**, **h**) and $n = 6$ (**e**). Data are representative (**a**, **b**, **d**–**f**, **h**) or compiled from (**j**, **k**) three independent experiments.

HuPBMS-NSG-SGM3 mice were rendered diabetic by multiple low-dose STZ treatment (MLD-STZ) and subsequently transplanted with wHILOs (Fig. 3a, b). Transplanted PD-L1$^+$ wHILOs provided sustained blood glucose control compared to those lacking PD-L1 expression, with human C-peptide levels correlating with the extent of glycaemic control (Fig. 3c, d). The rapid development of hyperglycemia upon surgical removal of the transplanted kidneys implicated graft-derived insulin as the primary effector (Fig. 3c). Subsequent analysis of the recovered grafts revealed a marked reduction in the number of insulin-expressing cells in the non-immune shielded wHILOs and a corresponding increase in human lymphocytes (Fig. 3e, f).

Epigenetic memory drives immune-tolerant wHILOs

PDL1 expression is induced by interferon-γ (IFN-γ) stimulation in several cell types as well as multiple cancers and pancreatic islets[22,23]; however, extended exposure to cytokines—including IFN-γ—is known to induce β-cell death and/or dedifferentiation[24]. To determine whether this pathway could be exploited to minimize host immune responses, we initially exposed human islets to IFN-γ. An increase of about 20-fold in *PDL1* (also known as *CD274*) expression was seen 12 h after IFN-γ treatment (Extended Data Fig. 9g). Equivalent experiments in wHILOs saw a similar induction, with IFN-γ inducing *PDL1* expression in both insulin-expressing and non-expressing cells (GFP$^+$ and GFP$^-$ cells, respectively; Fig. 4a). Dose-escalating studies in wHILOs identified maximum *PDL1* induction after 12 h exposure to 10 ng ml^{-1} IFN-γ (Extended Data Fig. 9h). Although a more limited 2 h exposure at 10 ng ml^{-1} was sufficient to induce *PDL1*, this expression was transient (Fig. 4b). Given that tolerance to inflammatory stimuli such as lipopolysaccharide has been associated with epigenetic changes, we investigated whether sequential IFN-γ stimulation could induce a sustained induction of *PDL1*. Indeed, repeated short exposures to IFN-γ (multiple pulse-stimulated (MPS)) led to sustained *PDL1* expression and concomitant increases in protein levels (Fig. 4c–e). Notably, GSIS functionality was not compromised by MPS IFN-γ exposure (Fig. 4f). Furthermore, MPS IFN-γ-treated wHILOs were protected against IL-1β-induced β-cell dedifferentiation, as revealed by the expression of β-cell identity markers *INS* and *UCN3* (Fig. 4g, h).

To provide mechanistic insight into the IFN-γ-driven changes in wHILOs, the genome-wide transcriptional changes induced by acute (12 h exposure) and MPS treatments were associated with alterations in chromatin accessibility, as measured by ATAC–seq. Largely overlapping gene sets were induced by the IFN-γ treatments that included *PDL1*, whereas approximately half of the downregulated genes were commonly affected (Extended Data Fig. 11a, b). Gene ontology of the commonly upregulated gene set identified IFN-γ pathways (data not shown). By contrast, pathways that reflect the cell inflammation status, including negative regulation of IL-1β production and inflammatory pathways were identified only in the MPS-upregulated gene set, whereas positive regulation of NF-κB signalling and apoptosis were

found selectively in the MPS-downregulated gene set (Extended Data Fig. 11c). Overlaying changes in chromatin accessibility revealed persistent increases at gene loci, including *PDL1*, *IRF9*, *JUNB* and *JUND* after MPS IFN-γ treatment, in agreement with the sustained increases in gene transcript levels (Extended Data Fig. 11d). By contrast, whereas increased accessibility was seen at IFN-γ-responsive genes, including *IRF1* and *STAT1*, after the acute treatment, these increases were not sustained in the MPS treatment (Extended Data Fig. 11d).

We investigated the utility of MPS IFN-γ treatment to generate immune-evasive wHILOs (wHILO^{ie}) in immune-competent, STZ-induced diabetic C57BL6J mice. Notably, transplantation of wHILO^{ie} reduced glucose levels for more than 40 days, whereas the efficacy of naive wHILOs (not exposed to IFN-γ) progressively decreased, in agreement with the reduced levels of human C-peptide in serum (Fig. 4i–k). Similar results were seen with transplantations in humanized diabetic mice, where surgical removal of the recipient kidney led to an abrupt loss of glycaemic control (Extended Data Fig. 12a, b). An increase in the number of insulin-expressing cells, accompanied by reduced lymphocyte infiltration and a decrease in the relative number of activated T helper cells ($CD4^+CD3^+$) was seen in the recovered wHILO^{ie} grafts (Extended Data Fig. 12c).

In sum, these results suggest that the MPS IFN-γ protocol induces an epigenetic memory that leads to cytokine tolerance and sustained de novo PD-L1 expression in wHILOs, and supports the utility of wHILO^{ie} as a therapy to alleviate insulin-dependent diabetes.

Discussion

A combination of genetic and environmental factors underlies the autoimmune destruction of β-cells, and although exogenous insulin provides glycaemic control, long-term complications associated with diabetes are a continuing concern. The ability to generate glucose-responsive human β-cells suitable for transplantation has the potential to substantially improve patients' lives. Here, building on previous work[1,3,4,25,26], we describe a protocol that systematically drives the differentiation of iPS cells to insulin-positive, glucose-responsive β-like cells. Adaptation of this program to 3D cultures facilitates the generation of metabolically mature, immune-evasive human islet-like organoids (wHILO^{ie}) capable of restoring glucose homeostasis in diabetic, immune-competent mice. Notably, the identification of WNT4 as a metabolic maturation factor enabled the production of functional HILOs in fully chemically defined medium (Fig. 1e, f).

A key challenge for stem cell-based therapeutics is autoimmune rejection of transplanted cells[27,28]. During antigen presentation, interactions between cytotoxic T-lymphocyte antigen-4 (CTLA-4) and B7 molecules, as well as programmed cell death protein 1 (PD-1) and its ligand PD-L1, negatively regulate immune responses in a non-redundant manner. Here we show that wHILOs overexpressing PD-L1 are protected from xenograft (Fig. 2d) and allogenic (Fig. 3c) rejection. Furthermore, immune-evasive HILOs with sustained, endogenous PD-L1 expression maintain glucose homeostasis in immune-competent as well as humanized diabetic mice.

Generating patient-derived insulin-producing cells has the potential to further reduce the risk of alloimmune rejection; however, clinical-grade autologous transplants will probably be prohibitively expensive[29]. Alternatively, allogenic transplantation of major histocompatibility complex (MHC)-matched grafts may reduce immune responses, although the threat from alloreactive T cells remains[30]. MHC matching, together with the induction of immune tolerance, may provide the most promising strategy for controlling immune responses, ideally without immunosuppressive drugs. Although insulin injections and glucose monitoring can effectively manage diabetes in the acute setting, this does not replace the multifunctional role of the islet. The generation of glucose-responsive, immune-evasive HILOs offers a physiologic alternative to current immune-suppressive cadaveric or device-dependent technologies.

Online content

Any methods, additional references, Nature Research reporting summaries, source data, extended data, supplementary information, acknowledgements, peer review information; details of author contributions and competing interests; and statements of data and code availability are available at https://doi.org/10.1038/s41586-020-2631-z.

1. Yoshihara, E. et al. ERRγ is required for the metabolic maturation of therapeutically functional glucose-responsive β cells. *Cell Metab.* **23**, 622–634 (2016).
2. Hrvatin, S. et al. Differentiated human stem cells resemble fetal, not adult, β cells. *Proc. Natl Acad. Sci. USA* **111**, 3038–3043 (2014).
3. Rezania, A. et al. Reversal of diabetes with insulin-producing cells derived in vitro from human pluripotent stem cells. *Nat. Biotechnol.* **32**, 1121–1133 (2014).
4. Pagliuca, F. W. et al. Generation of functional human pancreatic β cells in vitro. *Cell* **159**, 428–439 (2014).
5. Kieffer, T. J. Closing in on mass production of mature human beta cells. *Cell Stem Cell* **18**, 699–702 (2016).
6. Liu, J. S. & Hebrok, M. All mixed up: defining roles for β-cell subtypes in mature islets. *Genes Dev.* **31**, 228–240 (2017).
7. Takebe, T. et al. Vascularized and functional human liver from an iPSC-derived organ bud transplant. *Nature* **499**, 481–484 (2013).
8. Asai, A. et al. Paracrine signals regulate human liver organoid maturation from induced pluripotent stem cells. *Development* **144**, 1056–1064 (2017).
9. Bader, E. et al. Identification of proliferative and mature β-cells in the islets of Langerhans. *Nature* **535**, 430–434 (2016).
10. van der Meulen, T. et al. Urocortin3 mediates somatostatin-dependent negative feedback control of insulin secretion. *Nat. Med.* **21**, 769–776 (2015).
11. Blum, B. et al. Functional beta-cell maturation is marked by an increased glucose threshold and by expression of urocortin 3. *Nat. Biotechnol.* **30**, 261–264 (2012).
12. van der Meulen, T. et al. Urocortin 3 marks mature human primary and embryonic stem cell-derived pancreatic alpha and beta cells. *PLoS ONE* **7**, e52181 (2012).
13. Prentki, M., Matschinsky, F. M. & Madiraju, S. R. Metabolic signaling in fuel-induced insulin secretion. *Cell Metab.* **18**, 162–185 (2013).
14. Huang, S. M. et al. Tankyrase inhibition stabilizes axin and antagonizes Wnt signalling. *Nature* **461**, 614–620 (2009).
15. Baas, M. et al. TGFβ-dependent expression of PD-1 and PD-L1 controls $CD8^+$ T cell anergy in transplant tolerance. *eLife* **5**, e08133 (2016).
16. Martinov, T., Spanier, J. A., Pauken, K. E. & Fife, B. T. PD-1 pathway-mediated regulation of islet-specific $CD4^+$ T cell subsets in autoimmune diabetes. *Immunoendocrinology* **3**, e1164 (2016).
17. Keir, M. E. et al. Tissue expression of PD-L1 mediates peripheral T cell tolerance. *J. Exp. Med.* **203**, 883–895 (2006).
18. Ansari, M. J. et al. The programmed death-1 (PD-1) pathway regulates autoimmune diabetes in nonobese diabetic (NOD) mice. *J. Exp. Med.* **198**, 63–69 (2003).
19. Ma, D. et al. PD-L1 deficiency within islets reduces allograft survival in mice. *PLoS ONE* **11**, e0152087 (2016).
20. Rui, J. et al. β Cells that resist immunological attack develop during progression of autoimmune diabetes in NOD Mice. *Cell Metab.* **25**, 727–738 (2017).
21. Wang, C. J. et al. Protective role of programmed death 1 ligand 1 (PD-L1) in nonobese diabetic mice: the paradox in transgenic models. *Diabetes* **57**, 1861–1869 (2008).
22. Colli, M. L. et al. PDL1 is expressed in the islets of people with type 1 diabetes and is up-regulated by interferons-α and-γ via IRF1 induction. *eBioMedicine* **36**, 367–375 (2018).
23. Osum, K. C. et al. Interferon-gamma drives programmed death-ligand 1 expression on islet β cells to limit T cell function during autoimmune diabetes. *Sci. Rep.* **8**, 8295 (2018).
24. Eizirik, D. L. & Mandrup-Poulsen, T. A choice of death—the signal-transduction of immune-mediated beta-cell apoptosis. *Diabetologia* **44**, 2115–2133 (2001).
25. Russ, H. A. et al. Controlled induction of human pancreatic progenitors produces functional beta-like cells in vitro. *EMBO J.* **34**, 1759–1772 (2015).
26. Nair, G. G. et al. Recapitulating endocrine cell clustering in culture promotes maturation of human stem-cell-derived β cells. *Nat. Cell Biol.* **21**, 263–274 (2019).
27. Sneddon, J. B. et al. Stem cell therapies for treating diabetes: progress and remaining challenges. *Cell Stem Cell* **22**, 810–823 (2018).
28. Zhou, Q. & Melton, D. A. Pancreas regeneration. *Nature* **557**, 351–358 (2018).
29. Turner, M. et al. Toward the development of a global induced pluripotent stem cell library. *Cell Stem Cell* **13**, 382–384 (2013).
30. Morizane, A. et al. MHC matching improves engraftment of iPSC-derived neurons in non-human primates. *Nat. Commun.* **8**, 385 (2017).

Methods

Data reporting

No statistical methods were used to predetermine sample size. The experiments were not randomized. The investigators were not blinded to allocation during experiments and outcome assessment.

Maintenance of mouse lines

Animals were maintained in a pathogen-free animal facility on a 12 h:12 h light:dark cycle at an ambient temperature of 23 °C. Water and food were provided ad libitum. Experiments used 8–20-week-old age- and background-matched male C57BL/6J (stock no. 000664, Jackson Laboratory), NOD/SCID mice (NOD.Cg-Prkdcscid Il2rgtm1Wjl/SzJ, stock no. 005557, Jackson Laboratory), β cell-specific ERRγ-knockout mice[1], Hu-PBMC-SGM3 mice (referred to as humanized mice). Female NSG mice were injected with human PBMCs in NSG-SGM3 (Jackson 013062) strain and procedures were performed in accordance with protocols approved by the IACUC and Animal Resources Department of the Salk Institute for Biological Studies. Cohort sizes were determined empirically on the basis of initial studies. Littermates were randomly assigned to experimental arms. STZ-treated mice were grouped on the basis of serum glucose levels, and mice with the highest glucose levels were used for positive control experiments (that is, mouse and human islet transplantations). No experiment was blinded nor randomized. All experiments were conducted with sex, age and strain matched mice.

Cell lines

Human iPS cells were derived from HUVECs by the Salk Stem Cell Core. HEK293LTV (Cell Biolabs), HuES8 (Harvard University), H1ES (Wicells), and hiPS cell-derived β-like cells (Takara, ChiPSC12 and ChiPSC22) were routinely tested for mycoplasma contamination. No commonly misidentified cell lines were used.

Generation of human insulin reporter and PD-L1-overexpressing human iPS cell lines

To mark β-cell specification, human iPS cells derived from HUVECs were infected with a human insulin GFP reporter, as previously described[1,31]. To visualize endogenous insulin promoter activity, CRISPR–Cas9 genome editing was used to introduce GFP into the insulin promoter (Supplementary Table 2). PD-L1-expressing hiPS cells were generated by infecting them with a CD274 (PD-L1)-expressing lentivirus (abm, LV113090) with puromycin selection. The human UCN3 proximal promoter sequence (−1298 to +103) was introduced by In-Fusion cloning (Clontech) into the promoter-less pLV-Cherry-Picker1 backbone (Clontech, 632574) using the ApaI and NotI sites. Primer sequences for PCR amplification of the promoter sequence from genomic DNA were 5′-GTCCATGCTGATCCATCCTT-3′ (forward) and 5′-TGCTTCTCCGGTATTGTTCC-3′ (reverse). A dual-reporter line for human UCN3 mCherry and human insulin GFP (hINS-GFP-EF1α-Neo) was generated by usingthe lentivirus system in hiPS cells.

Virus production

Lentiviruses were produced using second- or third-generation lentiviral systems in HEK293LTV cell line (Cell Biolabs).

3D gellan gum culture medium

Aqueous solutions of low-acyl gellan gum (Kelcogel F GG-LA, Modernist Pantry, 0.3% w/v) were sterilized by autoclaving before dilution in mTeSR1 (StemCell Technologies) or Custom TeSR medium (final concentration 0.015%) and the addition of methylcellulose (R&D systems, final concentration 0.3%) and penicillin–streptomycin.

Human multicellular spheroids

Pancreatic endocrine cells were prepared from hiPS cells as previously described. In brief, HUVEC-derived hiPS cells, obtained from the Salk Stem Cell Core, were maintained on matrigel (BD Biosciences)-coated dishes in complete Stem TeSR Media at 37 °C in a humidified 5% CO_2 incubator. Before pancreatic differentiation, hiPS cells were infected with a human insulin reporter lentivirus (pGreenZero lenti reporter human insulin, System Biosciences) by Spinfection (800*g*, 1 h) and then the medium was changed to 100 ng ml^{-1} human activin (R&D Systems), 3 μM CHIR99021 (Selleckchem) in differentiation medium (800 ml DMEM/F12, 13.28 g BSA, 10 ml Glutamax, 560 mg $NaHCO_3$, 330 mg thiamine, 100 mg reduced glutathione, 3,300 mg Vitamin C, 14 μg selenium, 10 ml nonessential amino acids, 2 ml trace element B (25022Cl, Corning), 1 ml trace element C (25023Cl, Corning), 7 μl β-mercaptoethanol, 2 ml chemically defined lipid concentrate (DLC), 2 ml GABA, 2 ml LiCl, 129.7 μg palmitic acid (PA), Insulin 2 mg, made up to 1,000 ml) for 2 days and then 100 ng ml^{-1} human activin in differentiation media for another 2 days (stage 1, pancreatic endoderm). Subsequently, medium was replaced with differentiation medium with 1 μM dorsomorphin (Calbiochem), 2 μM retinoic acid (Sigma), 10 μM SB431542 and 1% B27 supplement for 7 days (stage 2). Medium was then replaced with differentiation medium with 10 μM forskolin (Sigma), 10 μM dexamethasone (Stemgent), 10 μM TGF-β RI Kinase inhibitor II/Alk5 inhibitor II (Calbiochem or Enzo), 10 μM nicotinamide (Sigma), 1 μM 3,3′,5-triiodo-L-thyronine sodium salt (T3) and 1% B27 supplement for 4–5 days (day15–day19, pancreatic endocrine progenitors). Medium was replaced every day (stage 1), and then every other day (stage 2 and stage 3). Primary HUVECs and hADSCs (Invitrogen or PromoCell) were cultured in 15-cm dishes with EBM Medium (Ronza, cc-3121) or MesenProRS Medium (GIBCO, 12747-010 or Preadipocyte Growth Medium Kit, C-27417), respectively at 37 °C in a humidified 5% CO_2 incubator. For co-culturing experiments, pancreatic endocrine progenitors derived from human iPS cells were treated with Accutase, while HUVECs and hADSCs were treated with TrypLE (GIBCO, 12604-013) and cells were collected into 50-ml tubes. hiPS cell endocrine progenitors (hiPSC-EPs) (1×10^6 cells), HUVECs (7×10^6 cells) and hADSCs (10^5 to 2×10^5 cells) were co-cultured in a single well of a 24-well plate with 300 μl of Matrigel. For MCS generation, hiPSC-EPs (day 15–day 21, 1×10^6 cells), HUVECs (7×10^6 cells) and hADSCs (10^5 to 2×10^5 cells) were co-cultured in 3D Kelco Gel Custom TeSR with 10 μM forskolin (Sigma), 10 μM dexamethasone (Stemgent), 10 μM TGF-β RI kinase inhibitor II/Alk5 inhibitor II (Calbiochem or Enzo), 10 μM nicotinamide (Sigma), 1 μM 3,3′,5-triiodo-L-thyronine sodium salt (T3) and 1% of B27 supplement, R428 (2 μM), zinc sulfate (10 μM) and N-Cys (1 mM). Medium was changed every other day, with islet-like clusters forming within a few days.

HILO cultures

The following base differentiation media were used for production of HILOs. S1 medium: MCDB131 500 ml, 50% D-(+)-glucose 550 μl, $NaHCO_3$ 1.23 g, fatty acid-free BSA 10 g, ITX-X 10 μl, GlutaMax 5 ml, ascorbic acid 22 mg, penicillin/streptomycin 5 ml; S2 medium: MCDB131 500 ml, 50% D-(+)-glucose 550 μl, $NaHCO_3$ 0.615 g, fatty acid-free BSA 10 g, ITX-X 10 μl, GlutaMax 5 ml, ascorbic acid 22 mg, penicillin/streptomycin 5 ml; S3 medium: MCDB131 500 ml, 50% D-(+)-glucose 550 μl, $NaHCO_3$ 0.615 g, fatty acid-free BSA 10 g, ITX-X 2.5 ml, GlutaMax 5 ml, ascorbic acid 22 mg, penicillin/streptomycin 5 ml; S4 medium: MCDB131 500 ml, 50% D-(+)-glucose 550 μl, $NaHCO_3$ 0.615 g, fatty acid-free BSA 10 g, ITX-X 2.5 ml, GlutaMax 5 ml, ascorbic acid 22 mg, penicillin/streptomycin 5 ml, heparin 5 mg, zinc sulfate 1.43 mg; S5 medium: MCDB131 500 ml, 50% D-(+)-glucose 2,660 μl, $NaHCO_3$ 0.877 g, fatty acid-free BSA 10 g, ITX-X 2.5 ml, GlutaMax 5 ml, ascorbic acid 22 mg, penicillin/streptomycin 5 ml, heparin 5 mg, zinc sulfate 1.43 mg. hiPS cells were cultured in Matrigel-coated plates. Single-cell suspensions were prepared using Accutase, washed in PBS, and collected by centrifugation (1,000–1,300 rpm for 5 min). Cells were re-suspended with 3D Kelco Gel Stem TeSR Base Media in the presence of the ROCK inhibitor (10 μM Y-27632, StemCell) for 5 to 7 days until spheroids reached 50–100 μm

diameter. Medium was then replaced with 0.015% Kelco gel containing 0.3% methylcellulose and supplemented with 100 ng ml^{-1} human activin A (R&D Systems), 3 μM CHIR99021 (Axon or Selleckchem) in differentiation medium (S1) for 1 day and then 100 ng ml^{-1} human activin in differentiation medium (S1) for another 2 days (stage 1, definitive endoderm). Subsequently medium was replaced with differentiation medium (S2) with 50 ng ml^{-1} FGF7 (R&D Systems) for 2 days, differentiation medium (S3) with 50 ng ml^{-1} FGF7, 0.25 μM SANT-1 (Sigma), 1 μM retinoic acid (Sigma), 100 nM LDN193189, 10 μM Alk5 inhibitor II and 200 nM of the α-amyloid precursor protein modulator TPB for 3 days, then 50 ng ml^{-1} FGF7, 0.25 μM SANT-1 (Sigma), 1 μM retinoic acid (Sigma), 100 nM LDN193189, 10 μM Alk5 inhibitor II and 100 nM of the α-amyloid precursor protein modulator TPB for 2 days. Subsequently medium was replaced with differentiation medium (S4) with 0.25 μM SANT-1, 50 nM retinoic acid, 100 nM LDN193189, 10 μM Alk5 inhibitor II, 1 μM T3 for 3 days. Subsequently medium was replaced with differentiation medium (S5) with 100 nM LDN193189, 100 nM γ-secretase inhibitor XX (GSiXX, Millipore), 10 μM Alk5 inhibitor II, 1 μM T3 for 7 days. Subsequently, medium was replaced with differentiation medium (S5) with 10 μM Trolox (Calbiochem), 2 μM R428 (Selleckchem), 1 mM *N*-acetyl cysteine, 10 μM Alk5 inhibitor II, 1 μM T3 for an additional 7–20 days. After confirmation of insulin expression by quantitative PCR or reporter activity (typically days 20–30), medium was changed to differentiation medium (S5) with 10 μM Trolox (Calbiochem), 2 μM R428 (Selleckchem), 1 mM *N*-acetyl cysteine, 10 μM Alk5 inhibitor II, 1 μM T3 and 100 ng ml^{-1} recombinant human WNT4 (rhWNT4) (R&D Systems) with or without the addition of laminins (LM-511/521 and LM-411/421) for 5–10 days.

WNT5A conditional medium

WNT5A-producing fibroblasts (ATCC CRL-2814) and control fibroblasts (ATCC CRL-2648) were cultured with DMEM containing 10% FBS and 1% penicillin/streptomycin (complete medium). Upon reaching confluency, cells were washed with PBS before incubation in complete medium for one week. Conditioned medium was subsequently collected, filtered through a 0.2-μm sterile filter, and frozen at −80 °C in 50-ml aliquots. Conditioned medium was mixed with differentiation medium (S5 with 10 μM Trolox, 2 μM R428, 1 mM *N*-acetyl cysteine, 10 μM Alk5 inhibitor II, 1 μM T3) at 1:1 ratio, then used to treat HILOs for 5–10 days.

PD-L1 induction in human islets and wHILOs

PD-L1 expression was induced by recombinant human IFN-γ (R&D Systems, 285-IF, 2–12 h treatment at 1–50 ng ml^{-1} final concentration). For acute treatment, wHILOs were treated with 10 ng ml^{-1} IFN-γ in the differentiation medium (S5 with 10 μM Trolox, 2 μM R428, 1 mM *N*-acetyl cysteine, 10 μM Alk5 inhibitor II, 1 μM T3 and 100 ng ml^{-1} rhWNT4) for 2 h. Cells were then washed twice with PBS before culturing in differentiation medium (S5 with 10 μM Trolox, 2 μM R428, 1 mM *N*-acetyl cysteine, 10 μM Alk5 inhibitor II, 1 μM T3 and 100 ng ml^{-1} rhWNT4) (single-pulse stimulation). IFN-γ exposure was repeated 3 times with washing and 24 h resting time in differentiation medium (S5 with 10 μM Trolox, 2 μM R428, 1 mM *N*-acetyl cysteine, 10 μM Alk5 inhibitor II, 1 μM T3 and 100 ng ml^{-1} rhWNT4) between each IFN-γ exposure (MPS stimulation) to generate wHILO (MPS). After the final IFN-γ pulse, cells were cultured in the tissue culture incubator for a week before the RNA-seq analyses (Extended Data Fig. 11a–c), ATAC–seq analyses (Extended Data Fig. 11d) and the transplantation into STZ-induced diabetic C57BL6J mice (Fig. 4j) or humanized mice (Extended Data Fig. 12b).

Isolation of pancreatic islets

Mouse pancreatic islets were isolated as previously described[32] with slight modifications. In brief, 0.5 mg ml^{-1} collagenase P (Roche REF11213873001, diluted in HBSS buffer, GIBCO, 14170-112) was injected through the common bile duct, and the perfused pancreas dissected and incubated at 37 °C for 21 min. Digested exocrine cells and intact islets were separated via centrifugation over Histopaque-1077 (Sigma, H8889, 900x*g* for 15 min), and intact islets manually selected. Human islets were provided by the Integrated Islets Distribution Program under an approved protocol.

Insulin/C-peptide secretion assays

Insulin release from intact islets was monitored as previously described[1]. In brief, overnight-cultured isolated pancreatic islets (RPMI-1640 supplemented with 10% (v/v) fetal bovine serum and 1% (v/v) Antibiotic-Antimycotic (Gibco)) were pre-cultured at 37 °C for 30 min (Krebs-Ringer bicarbonate buffer (KRBB) containing 129.4 mM NaCl, 3.7 mM KCl, 2.7 mM $CaCl_2$, 1.3 mM KH_2PO_4, 1.3 mM $MgSO_4$, 24.8 mM $NaHCO_3$ (equilibrated with 5% CO_2, 95% O_2, pH7.4), 10 mM HEPES and 0.2% (v/v) BSA (fraction V, Sigma) with 3 mM glucose). Pancreatic islets were incubated in Krebs-Ringer bicarbonate HEPES buffer (KRBH) buffer (500 μl/10 islets) with 3 mM or 20 mM glucose for 30 min, the islets were pelleted, and secreted insulin levels determined in the medium by ELISA (Rat/mouse Insulin ELISA KIT (Millipore) and ultrasensitive human Insulin ELISA KIT or ultrasensitive human C-peptide ELISA Kit (Mercodia) for mouse and human islets, respectively). Human iPS cell-derived cells (1×10^6 cells per well in 24 well) were pre-cultured in 3 mM glucose KRBH buffer (500 μl per well). Cells were then incubated in KRBB (200 μl per well) with 3 mM or 20 mM glucose for 30 min, and C-peptide levels determined in the medium by human C-peptide ELISA KIT (Millipore) after pelleting of the cells. For 3D cultured HILOs, size matched (100–300 μm diameter) HILOs were pre-cultured with KRBH buffer with 3 mM glucose for 30 min before incubated in KRBH buffer (500 μl/20 HILOs) with 3 mM or 20 mM glucose for 30 min. Secreted human C-peptide or human insulin levels were measured in the medium by ELISA ultrasensitive (human Insulin ELISA KIT or ultrasensitive human C-peptide ELISA Kit (Mercodia)).

Oxygen consumption and extracellular acidification rates

OCR and extracellular acidification rate were recorded in 24-well plates using an XF24 Seahorse (Seahorse Biosciences). In brief, 70 size-matched human islets, hiPS cell spheroids, or HILOs were pre-cultured in 3 mM glucose XF DMEM medium (pH 7.4) with 1 mM sodium pyruvate (Base medium) for 1 h before transfer to XF24 islet culture plates in base medium. OCRs (reported as percent change compared to 3 mM glucose) were recorded during the incremental addition of glucose, up to a final concentration of 20 mM glucose. Subsequently, mitochondrial stress reagents (oligomycin, FCCP, rotenone and antimycin A), were added as instructed in the Mitostress Kit (Seahorse Biosciences).

Islet and HILO transplantation studies

Immunodeficient NOD/SCID, C57BL6J and Hu-PBMC-SGM3 mice were purchased from Jackson Laboratory and maintained in autoclaved cages in a SPF facility at the Salk Institute. Mice were rendered diabetic by a single high-dose (180 mg kg^{-1}) or 5 multiple low-dose (MLD, 50 mg kg^{-1}) injection of STZ (intraperitoneal, Sigma S0130–500MG). One week after STZ injection, mice with blood glucose levels higher than 300 mg dl^{-1} were used as transplant recipients. Human and mouse islets (200–500 islets or 500–1,000 islet equivalents for mouse islets, 500–1,000 islets or 1,000–2,000 islet equivalents for human islets per mouse) or HILOs (500 clusters) were resuspended in 200 μl RPMI-1640 medium, loaded into laboratory tubing (SiLastic, 508-004), and centrifuged (400*g* for 1–2 min) to generate cell clusters in the centre of the tubing. Cell clusters (~30–50 μl) were transplanted under the kidney capsules in 8–16 week old STZ-injected diabetic mice. Ketamine (80 mg kg^{-1}) and xylazine (10 mg kg^{-1}) were used as surgical anaesthetics and mice were placed on 37 °C heating pads to recover. Blood glucose was monitored using a Nova Max Plus. Nephrectomies for graft-removal experiments were carried out to confirm the efficacy for glucose regulation in the

transplanted wHILOs. The kidney with graft was ligated at the renal hilum using 4-0 silk (LOOK, SP116), and then resected. Removed grafts were processed for analyses of immune profiling.

ATAC–seq

ATAC–seq was performed on 50,000 GFP$^+$ cells purified using fluorescence-activated cell sorting (FACS) from HILOs treated with PBS or 100 ng ml^{-1} rhWNT4 from day 27 to day 34, as described[33]. Reads were aligned by Bowtie to hg19 and peaks were called by Homer using the default settings. Differential peaks and motif analyses from two biological duplicates were identified using HOMER[34]. Detailed methods for HOMER are freely available at http://homer.salk.edu/homer/. In brief, the program searches against the target and background sequences for enrichment of known motifs, returning motifs enriched with a threshold of 1.5 fold change and *P*-value less than 0.05. Promoter regions, defined as 1 kB upstream from the transcription start site, of genes with enhanced chromatin accessibility upon WNT4 treatment, were interrogated for enriched motifs of 8–16 bp using HOMER motif analysis.

Bulk RNA-seq library generation

Total RNA was isolated from cell pellets treated with RNAlater (Invitrogen) using the RNeasy micro kit (Qiagen) and treated with DNaseI (Qiagen) for 30 min at room temperature. Sequencing libraries were prepared from 100–500 ng total RNA using the TruSeq RNA Sample Preparation Kit v2 (Illumina) according to the manufacturer's protocol. In brief, mRNA was purified, fragmented, and used for first- and second-strand cDNA synthesis followed by adenylation of 3′ ends. Samples were ligated to unique adapters and PCR amplified. Libraries were then validated using the 2100 BioAnalyzer (Agilent), normalized and pooled for sequencing.

High-throughput sequencing and analysis

RNA-seq libraries prepared from 3 biological replicates for each experimental condition were sequenced on the Illumina HiSeq 2500 using bar-coded multiplexing and a 100-bp read length. Image analysis and base calling were automatically generated withthe Illumina HiSeq Real-Time Analysis Software. This yielded a median of 29.9 million usable reads per sample. Short read sequences were mapped to a UCSC hg19 reference sequence using the RNA-seq aligner STAR[35]. Known splice junctions from hg19 were supplied to the aligner and de novo junction discovery was also permitted. Differential gene-expression analysis, statistical testing and annotation were performed using Cuffdiff 2 (ref. [36]). Transcript expression was calculated as gene-level relative abundance in fragments per kilobase of exon model per million (FPKM) mapped fragments and employed correction for transcript abundance bias[37]. RNA-seq results for genes of interest were also explored visually using the UCSC Genome Browser. Heat maps were generated by R-Script with heatmap.2 (gplot) software or Cluster with Javatree view software. Scale of heat maps was determined by *Z*-score.

Droplet-based single-cell RNA sequencing

Three biological replicates (200 clusters per replicate) of hiPS cell-derived endocrine progenitors (day 15), HILOs, and WNT4-treated HILOs (100 ng ml^{-1} rhWNT4 for 5 days), as well as human islets (IIDP donor ID 1874) were dissociated into single-cell suspension using TrypLE. Single cells were processed through the Chromium Single Cell Platform using the GemCode Gel Bead, Chip and Library Kits (10X Genomics) as per the manufacturer's protocol. In brief, 8,800 single cells were sorted into 0.4% BSA in PBS for a targeted 5,000-cell recovery. Cells were transferred into Gel Beads (Chromium Single Cell 3′′ v2) in emulsion in the Chromium instrument, where cell lysis and barcoded reverse transcription of RNA occurred, followed by amplification, shearing and 5′ adaptor and sample index attachment. Libraries were sequenced on an Illumina HiSeq 4000.

scRNA-seq data analysis

Initial data processing, including de-multiplexing, alignment to the GRCh38 reference transcriptome from 10X Genomics and unique molecular identifier (UMI)-collapsing, were performed using Cell Ranger software (10x Genomics, v.2.0.2). An overview of sample information was generated from the results of Cell Ranger pipelines (Supplementary Table 3). R studio (https://www.rstudio.com/), Cell Ranger R Kit, Seurat and other custom R scripts were used. Clustering of cells was performed using the Seurat R package in two iterative rounds of principal component analysis. Cells with unique gene counts less than 200 and anomalously high mitochondrial gene expression (cells with >10% mitochondrial genes) were removed (FilterCells function) before normalization of digital gene expression matrices by total expression, multiplied by a scale factor (default setting of 10,000) and log-transformed (NormalizeData function). A set of variable genes were then identified by binning the average expression of all genes and dispersion (variance divided by the mean) for each gene, placing these genes into bins, and then calculated *z*-score for dispersion within each bin (FindVariableGenes Function). Linear dimensional reduction was performed using the default setting of RunPCA and the principal components were evaluated for statistically significant gene expression signals using the Jackstraw method (JackStraw function, data not shown). At most, 12 principal components were used in this second round of clustering. *t*-SNE mapping was used to visualize scRNA-seq results. Clustered cell populations were classified and the top 10 differentially expressed genes identified (*FindAllMarkers* function). Cell types within the clustered populations were verified by the expression of canonical marker genes including genes for insulin (β cells), glucagon (α cells), somatostatin (δ cells), pancreatic polypeptide (γ cells), ghrelin (ε cells), *PRSS1* (acinar cells), *KRT19* (duct cells) and *ACTA2* (stellate cells). scRNA-seq data from WNT4-treated HILOs (4,840 cells) and human islets (7,248 cells) were combined in 1 Seurat object and the highly variable genes were identified as described above. Cell types within the clustered populations were identified by reference to differentially expressed genes in human islet cells. Seurat FindIntegrationAnchors and IntegrateData functions with canonical correlation analysis were used to integrate datasets including HILO, wHILO and human islets, and gene expression count was restored with single-cell analyses via expression recovery (SAVER). Differentially expressed genes between wHILOs and human islets in each defined cluster were identified using FindMarkers (Seurat v.2.0). Default Seurat settings were used to examine the expression in single cells in clusters. *ESRRG*- and insulin-positive cells were extracted using WhichCells (expression cut-off >0.1), and violin plots generated using VlnPlot function.

All parameter settings including minimum number of read and minimum gene number are specified in Supplementary Table 2. We used MAGIC[38] to impute gene expression data in the matrices from the Seurat object. Rmagic (R package for MAGIC) was implemented with the recommended t settings from its GitHub repository (including optimal *t* selection, $t = 4$, $k = 60$, npca = 20). The restored matrix of expression was used to examine gene expression and fold-changes using violin plots and heat maps. To identify significant gene changes among multiple datasets, double positive cells (for example, *ESRRG* and *INS*) were filtered out using the WhichCells function after RunALRA (Seurat v.3 wrappers). Detailed violin plot statistics for Extended Data Figs. 2d, 8b, i are provided in Supplementary Table 5.

Software and program for bioinformatics analysis

The software or programs used for genomic data analysis were R studio (https://www.rstudio.com/), Cell Ranger R Kit (https://support.10xgenomics.com/single-cell-gene-expression/software/pipelines/latest/rkit), Seurat (https://satijalab.org/seurat/)[39,40], DAVID (https://david.ncifcrf.gov/home.jsp)[41], GOplot (https://wencke.github.io)[42], UCSC

genome browser (http://genome.ucsc.edu)[34] and Homer (http://homer.ucsd.edu/homer/).

Immunohistochemistry

Immunohistochemistry of frozen or paraffin-embedded sections of pancreas, human islets, and human islet-like organoids (HILOs) was performed with antibodies to insulin (1/100, Abcam ab7842), C-peptide (1/100, Abcam ab30477), glucagon (1/100, Abcam ab10988), somatostatin (1/100, Abcam ab103790), pancreatic polypeptide (1/100, Abcam, ab113694), NKX2-2 (1/100, DSHB, 74.5A5), NKX6-1 (1/100, DSHB, F55A12), MAFA (1/100, Abcam, ab26405), MAFB (1/100, Abcam, ab66506 and 1/100, Bethyl Laboratories, A700-046), PDX-1 (1/100, R&D, AF2419), CHGA (1/100, Abcam, ab15160), synaptophysin (1/100, Biogenex, MU363-UC) and PD-L1 (1/100, Abcam, ab20592). For MAFA and MAFB, signal amplification was performed using poly-HRP secondary antibody (Thermo Scientific, B40962) and TSA-Cy3 kit (Akoya Biosciences, SAT704A001EA). Secondary antibodies were coupled to Alexa Fluor 568 or Alexa Fluor 647 (Life Technologies) and visualized by confocal microscopy (ZEISS) or fluorescence microscopy. Hoechst 33342 (Thermo Scientific, 62249, 1 μg ml^{-1} final concentration) was used for nuclear staining.

Flow cytometry

Clusters at indicated stages were dissociated with TrypLE (GIBCO) with 20 μg ml^{-1} DNase for 12 min at 37 °C and then fixed with 4% PFA for 10 min at room temperature. Clusters were then permeabilized with 0.2% Triton X-100 for 10 min, blocking with 10% goat serum for 30 min and stained for various intracellular markers with antibodies, C-peptide, (1/100, abcam, ab30477), PDX-1 (1/100, BD, 562161), NKX6-1 (1/100, BD, 563338), chromogranin A (1/100, BD, 564583), MAFA (1/100, abcam, ab26405), MAFB (1/100, abcam, ab66506), glucagon (1/100, abcam, ab82270), somatostatin (1/100, abcam, 108456) for analysis using a BD Biosciences LSRII. Data were analysed by FlowJo software. Secondary antibodies for C-peptide, glucagon and somatostatin were coupled to Alexa Fluor 647 (Life Technologies).

Electron microscopy analyses

Human islets and HILOs were pelleted in 2% low-melting-point agarose and subsequently fixed in 2.5% glutaraldehyde with 2% paraformaldehyde in 0.15 M cacodylate buffer containing 2 mM calcium chloride (pH 7.4) for 1 h at 4 °C. Excess agarose was removed and the pellet was washed in buffer before secondary fixing in 1% osmium tetroxide/0.3% potassium ferrocyanide in buffer. After washing in water, the pellet was en bloc stained with 2% uranyl acetate followed by graded dehydration in ethanol (35%, 50%, 70%, 90%, 100% and 100%). Samples were then rapidly infiltrated in Spurr's resin using a Pelco BioWave microwave processing unit (Ted Pella), embedded in Pelco Pyramid tip mould (Ted Pella), and cured at 60 °C overnight. Ultrathin sections (70 nm) were cut on a Leica UC7 ultramicrotome (Leica) and examined on a Libra120 (Zeiss) at 120V.

Immune profiling of transplanted HILOs

Transplanted HILOs were collected 26 days after transplantation and dissociated into single cells using TrypLE. The cells were stained by Zombie-UV staining Dye (BioLegend, 77474) to assess live or dead status. After blocking common epitopes found in extracellular regions of mouse Fc receptors by Fc block (Anti-mouse CD16/CD32 (Fc Shield) (70-0161-U500) staining, antibodies (1:100 dilution) to the cell surface markers CD19 (PerCP/Cy5.5 anti-mouse CD19, BioLegend, 115533), Nk1.1 (anti-mouse Nk1.1 PE, eBioscience, 12-5941-81), CD45 (Brilliant Violet 510 anti-mouse CD45, BioLegend, 103138), CD3 (Brilliant Violet 650 anti-mouse CD3, BioLegend, 100229) and Cd11b (anti-human/mouse APC-cyanine, TONBO, 25-0112U100) were used for FACS-based immune profiling. For flow cytometry analyses, data were collected using a BD Biosciences LSRII. For cell sorting, a BD Influx was used (100-μm nozzle tip and 1× PBS sheath fluid with sheath pressure set to 18.5 psi) with sample and collection cooling set to 4 °C. Viable (Zombie-UV dye negative) single cells were selected for FACS or analyses using forward scatter (FSC) and side scatter (SSC) gating, followed by pulse-width discrimination for FSC and SSC.

Quantitative PCR analysis

Total RNA was extracted using TRIzol (Invitrogen) and RNeasy (Qiagen). Reverse transcription was performed with a SuperScript III First-Strand Synthesis System (Invitrogen) or PrimeScript RT reagent kit (TAKARA). Real time quantitative PCR with reverse transcription (RT–qPCR) was performed using SYBR Green (Bio-Rad). Primer information is provided in Supplementary Table 4.

Statistics and reproducibility

Data analysis was performed using GraphPad Prism v.7 or Microsoft Excel. Results are expressed as the mean ± s.e.m. Statistical comparisons were made using Student's paired *t*-test. Statistically significant differences are indicated as $^{*}P < 0.05$, $^{**}P < 0.01$ or $^{***}P < 0.001$. The sample size (*n*) indicates the total number of independent biological samples. Experimental and technical triplicates were performed for all RT–qPCR analyses. HILO generation in 3D cultures was performed more than 50 times. For in vitro GSIS (Fig. 1g, Extended Data Fig. 3e, f, j) and in vivo transplantation studies (Figs. 2d, 3c, 4j, Extended Data Figs. 3k, 12b), GFP and *INS* ($C_t < 20$), *UCN3* ($C_t < 28$), *MAFA* ($C_t < 30$), *ESRRG* ($C_t < 30$) expression in HILOs was confirmed before the experiments.

Reporting summary

Further information on research design is available in the Nature Research Reporting Summary linked to this paper.

Data availability

RNA-seq and ATAC–seq data that support the findings of this study have been deposited in the National Center for Biotechnology Information Sequence Read Archive database under accession no. PRJNA505532. Source data are provided with this paper.

31. Wei, Z. et al. Vitamin D switches BAF complexes to protect β cells. *Nat. Commun.* **173**, 1135–1149 (2018).
32. Yoshihara, E. et al. Disruption of TBP-2 ameliorates insulin sensitivity and secretion without affecting obesity. *Nat. Commun.* **1**, 127 (2010).
33. Buenrostro, J. D., Wu, B., Chang, H. Y. & Greenleaf, W. J. ATAC-seq: a method for assaying chromatin accessibility genome-wide. *Curr. Protoc. Mol. Biol.* **109**, 21.29.1–21.29.9 (2015).
34. Heinz, S. et al. Simple combinations of lineage-determining transcription factors prime *cis*-regulatory elements required for macrophage and B cell identities. *Mol. Cell* **38**, 576–589 (2010).
35. Dobin, A. et al. STAR: ultrafast universal RNA-seq aligner. *Bioinformatics* **29**, 15–21 (2013).
36. Trapnell, C. et al. Differential analysis of gene regulation at transcript resolution with RNA-seq. *Nat. Biotechnol.* **31**, 46–53 (2013).
37. Roberts, A., Pimentel, H., Trapnell, C. & Pachter, L. Identification of novel transcripts in annotated genomes using RNA-seq. *Bioinformatics* **27**, 2325–2329 (2011).
38. van Dijk, D. et al. Recovering gene interactions from single-cell data using data diffusion. *Cell* **174**, 716–729 (2018).
39. Macosko, E. Z. et al. Highly parallel genome-wide expression profiling of individual cells using nanoliter droplets. *Cell* **161**, 1202–1214 (2015).
40. Butler, A., Hoffman, P., Smibert, P., Papalexi, E. & Satija, R. Integrating single-cell transcriptomic data across different conditions, technologies, and species. *Nat. Biotechnol.* **36**, 411–420 (2018).
41. Huang da. W. et al. Extracting biological meaning from large gene lists with DAVID. *Curr. Protoc. Bioinformatics* Ch. 13, https://doi.org/10.1002/0471250953.bi1311s27 (2009).
42. Walter, W., Sánchez-Cabo, F. & Ricote, M. GOplot: an R package for visually combining expression data with functional analysis. *Bioinformatics* **31**, 2912–2914 (2015).

Acknowledgements We thank J. Norris, H. Song, B. Henriquez, B. Collins and H. Juguilon for technical assistance; L. Ong and C. Brondos for administrative assistance; and M. Ahmadian and S. Liu for sharing materials and helpful discussion. scRNA-seq and ATAC–seq were supported by Next Generation Sequencing Core (N. Hah) of the Salk Institute and the UCSD IGM Genomics Center (K. Jepsen). Cell sorting and flow cytometry analyses, TEM and stem cell cultures were supported by the Flow Cytometry Core, the Waitt Advanced Biophotonics Core and the Stem Cell Core facilities at the Salk Institute, with funding from NIH-NCI CCSG: P30 014195, S10-OD023689, and the Waitt Foundation. R.M.E. is an

investigator of the Howard Hughes Medical Institute at the Salk Institute and March of Dimes Chair in Molecular and Developmental Biology. This work is supported by grants from CIRM (DISC2-11175), NIH (1RO1DK120480-01), the Glenn Foundation for Medical Research, the Leona M. and Harry B. Helmsley Charitable Trust (2017-PG-MED001), Ipsen/Biomeasure, and by a gift from Steven and Lisa Altman. C.L. and M.D. are funded by grants from the National Health and Medical Research Council of Australia Project (512354, 632886, and 1043199). E.Y. is supported by DRC P&F grant (P30 DK063491), and Z.W. is supported by NIH (1K01DK120808). We dedicate this work to the memory of our inspirational friend and colleague Maryam Ahmadian.

Author contributions E.Y. conceived and designed the study; E.Y., C.O., E.G., Z.W., T.G.O., T.W.T., D.W., F.C., Y.D., R.T.Y. and C.L. performed experiments; E.Y., C.O., E.G., Z.W., T.G.O., R.T.Y., C.L., A.R.A., M.D. and R.M.E analysed data. E.Y., M.D. and R.M.E. supervised the study, and E.Y., R.T.Y., A.R.A., M.D. and R.M.E. prepared the manuscript.

Competing interests The authors declare no competing interests.

Additional information

Supplementary information is available for this paper at https://doi.org/10.1038/s41586-020-2631-z.

Correspondence and requests for materials should be addressed to R.M.E.

Peer review information *Nature* thanks Anne Grapin-Botton, Heiko Likert and the other, anonymous, reviewer(s) for their contribution to the peer review of this work.

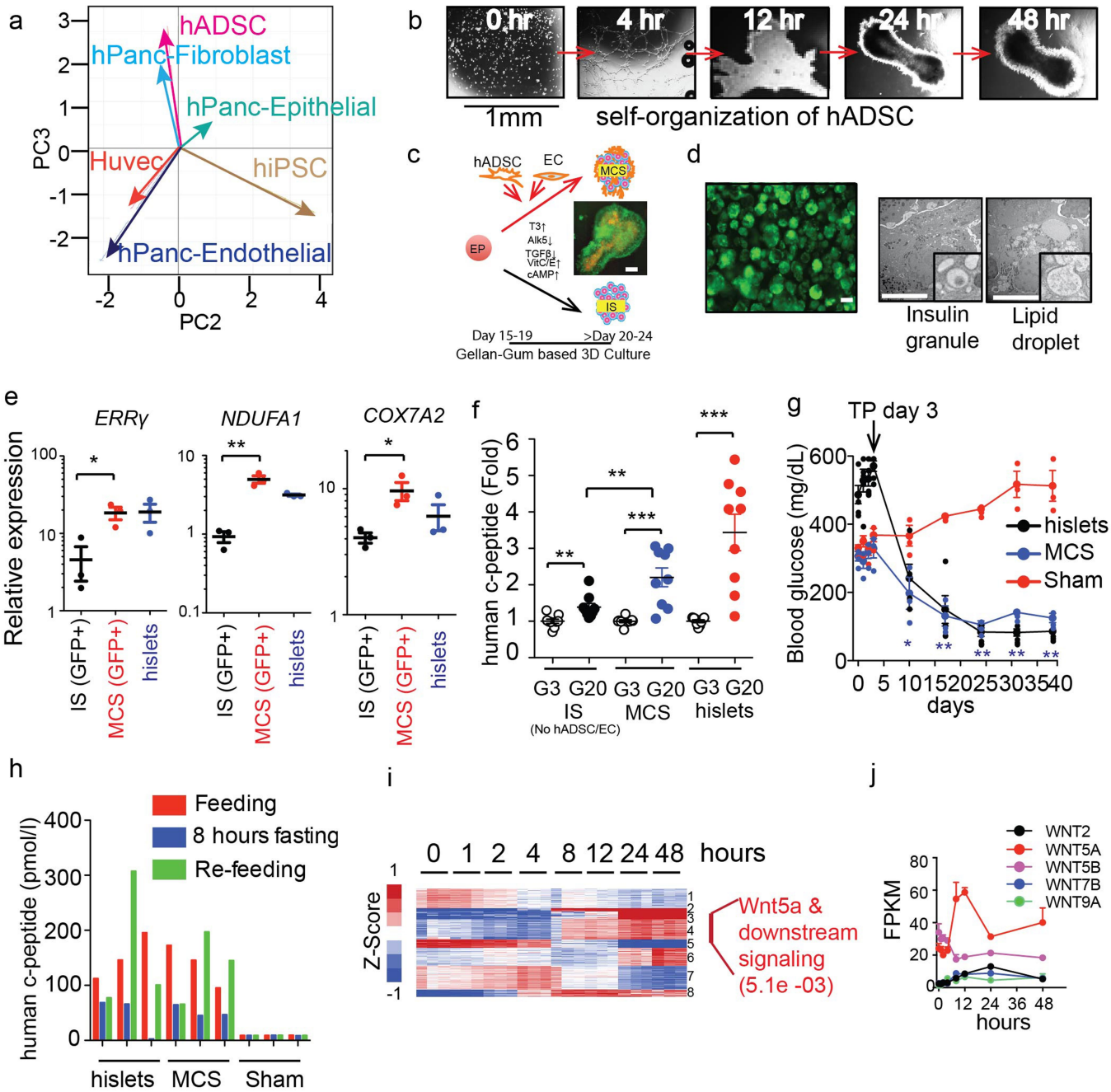

Extended Data Fig. 1 | Cellular crosstalk drives functional maturation of hiPSC-derived β-like cells. a, Principal component analysis of transcriptomes from human iPSCs (hiPSCs), primary human pancreatic epithelial cells (hPanc Epithelial), human adipose-derived stem cells (hADSCs), human pancreatic fibroblasts (hPanc Fibroblast), human umbilical vein endothelial cells (HUVECs) and human pancreatic microvascular endothelial cells (hPanc Endothelial) ($n = 3$). **b**, Time course of human adipose-derived stem cell (hADSC) culture in Matrigel (1:1 dilution in hADSC media, 2 million cells in 300 µl) showing intrinsic self-organization. Scale bar 1 mm. **c**, Schematic for multicellular islet-like spheroids (MCS) and islet-like spheroid (IS) generation. hiPSC-derived endocrine progenitors were co-cultured with hADSC and endothelial cells (EC, HUVECs) in gellan gum-based 3D culture system (left). MCS generated in Matrigel showing the incorporation of ECs (Lentivirus-mCherry expression) and insulin expression (Lentivirus-GFP, right). Scale bar 100 µm. **d**, MCS cultured in 3D gellan gum system showing insulin expression (Lentivirus-GFP, upper panel). Electron microscopy images of MCS showing insulin granules (lower right) and lipid droplets in hADSC (lower right). **e**, Gene expression in sorted insulin-expressing cells (GFP^+) from IS, MCS, or human islets (hislets) ($n = 3$). **f**, Human C-peptide secretion in response to 3 mM (G3) or 20 mM (G20) glucose from IS, MCS and hislets ($n = 9$). **g**, Random fed blood glucose levels in STZ-induced diabetic NOD/SCID mice after sham treatment or transplantation of MCS (500) or human islets ($n = 3, 3$ and 5 respectively). **h**, Serum human C-peptide levels during feeding, fasting, and refeeding cycles in mice 4 weeks after transplantation ($n = 3$ per group). **i**, Heat map of expression changes during hADSC culture in Matrigel (left). Most significantly affected gene ontology category in indicated gene clusters (right) ($n = 3$). **j**, Temporal expression of *WNTs* during hADSC self organization shown in **b** ($n = 3$). Error bars represent ± s.e.m. $^*P < 0.05$, $^{**}P < 0.01$, $^{***}P < 0.001$, one-tailed, Student's paired *t*-test. Data representative of 3 independent experiments (**b**, **d**–**g**) or experimental triplicates (**a**, **h**–**j**).

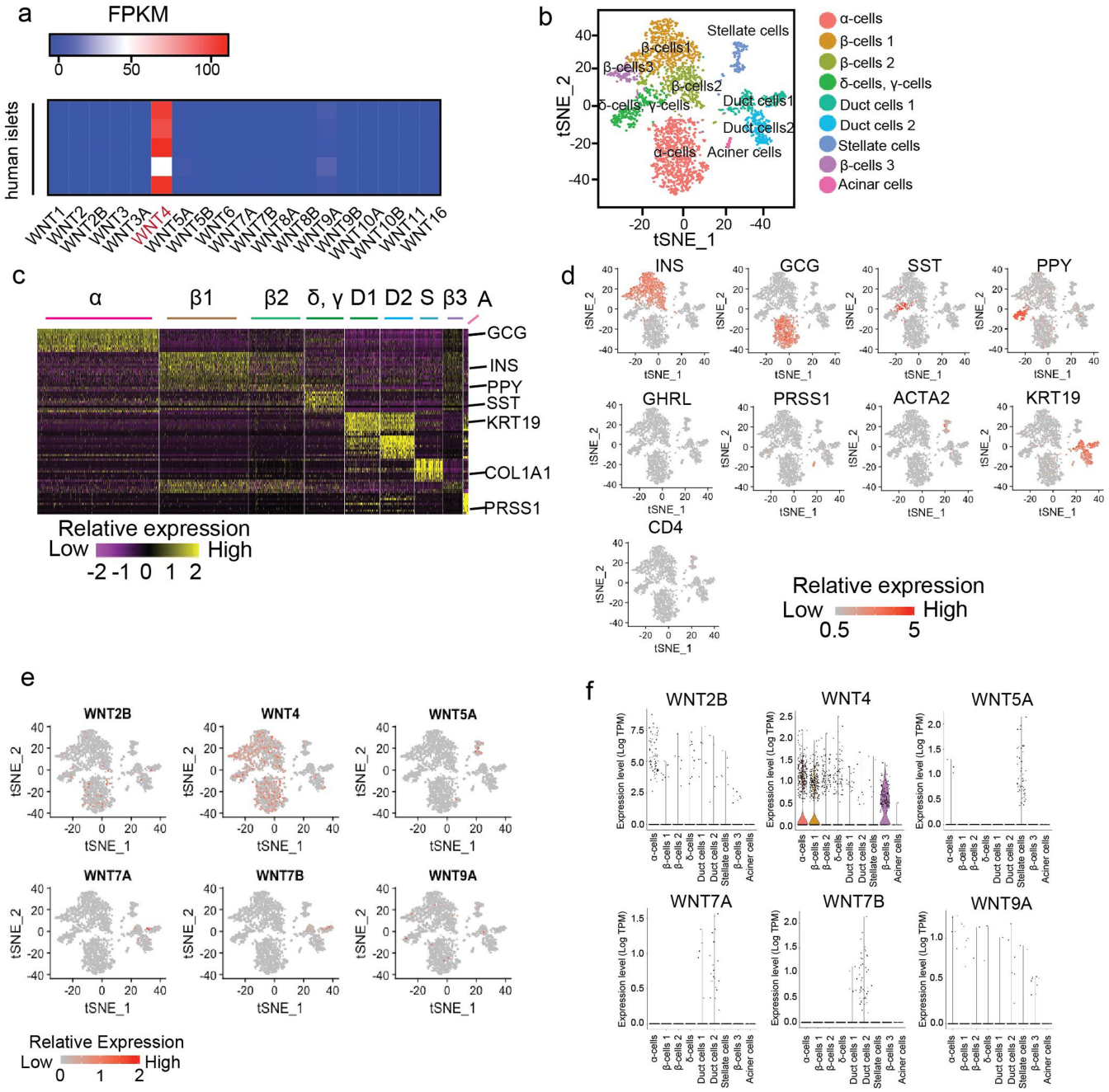

Extended Data Fig. 2 | WNT expression in human islets. a, Heat map of relative expression of *WNTs* in human islets ($n = 5$). **b**, *t*-SNE clustering of human islet single cell transcriptomes ($n = 3,245$). Annotated cell types assigned based on known marker gene expression. **c**, Heat map of expression of top 10 signature genes in human islet cell clusters from **b**. **d**, Single cell expression of signature hormonal and cell type-specific genes in human islets. **e**, **f**, Single cell (**e**) and violin plots (**f**) of *WNT2B*, *WNT4*, *WNT5A*, *WNT7A*, *WNT7B* and *WNT9A* expression in human islets, statistics provided in Supplementary Table 5. Data from 3 pooled human islets (**b**–**f**).

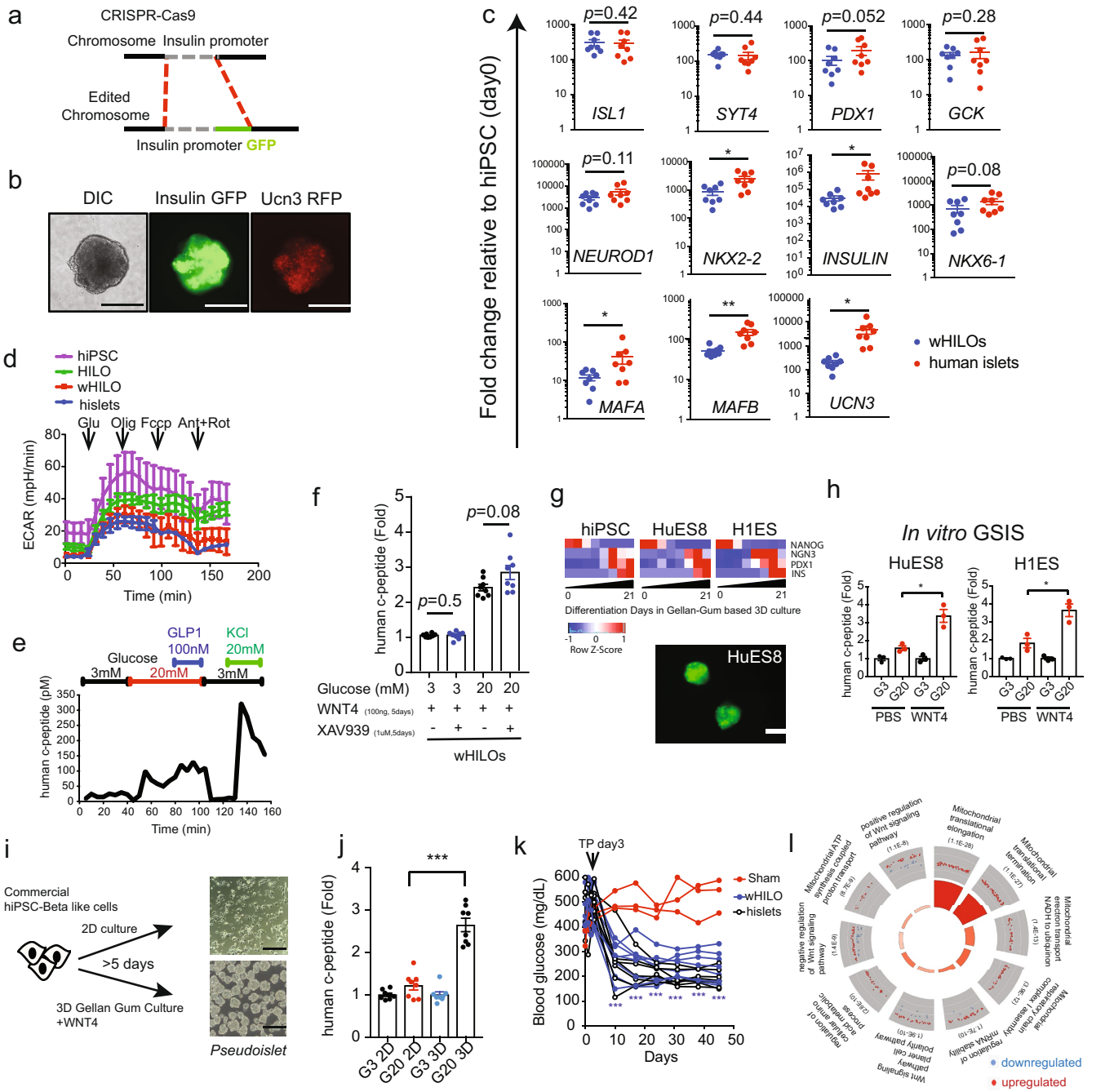

Extended Data Fig. 3 | Phenotypic and genotypic characterization of HILOs. a, Schematic of CRISPR–Cas9 knock-in for endogenous human insulin promoter-driven GFP expression in hiPSC. **b**, Representative differential interference contrast (DIC) images of wHILOs with insulin-GFP and UCN3-RFP expression (scale bar, 100 µm, $n = 3$). **c**, Relative expression of *ISL1*, *SYT4*, *PDX1*, *GCK*, *NEUROD1*, *NKX2-2*, *INS*, *NKX6-1*, *MAFA*, *MAFB* and *UCN3* in wHILOs and human islets determined by qPCR ($n = 8$ per sample type). **d**, Extracellular acidification rate (ECAR) measured in day 0 hiPSC spheroids (purple), PBS-treated HILOs (green), WNT4-treated HILOs (red) and human islets (blue) ($n = 3$). **e**, Kinetics of human C-peptide secretion from WNT4-treated HILOs in response to progressive exposure to 3 mM glucose, 20 mM glucose, 20 mM glucose + 100 nM GLP-1, 3 mM glucose, and 3 mM glucose + 20 mM KCl. **f**, Glucose-stimulated human C-peptide secretion from wHILOs treated with and without XAV939 to promote β-catenin degradation (XAV939, 1 µM for 3 days) ($n = 8$). **g**, Temporal gene expression (*NANOG*, *NGN3*, *PDX1*, *INS*) during differentiation of hiPS, HUES8 and H1ES cells to HILOs (upper panel). Insulin-driven GFP expression in day 21 HILOs derived from HUES8 (lower panel, scale bar 100 µm). **h**, In vitro C-peptide secretion in response to 3 mM (G3) and 20 mM (G20) glucose in wHILOs from HUES8 and H1ES ($n = 3$). **i**, Schematic depicting culture conditions for commercially available hiPSC-derived β-like cells (left) and light microscopy image of cultured cells (right, scale bar 100 µm). **j**, In vitro C-peptide secretion in response to 3 mM (G3) and 20 mM (G20) glucose from cultures described in **i** ($n = 8$). **k**, Blood glucose levels in STZ-induced diabetic NOD/SCID mice. Transplantation (TP) of 500 wHILOs, hislets, or sham surgery was performed at day 3 ($n = 7$, 6, and 3, respectively). **l**, Gene ontology of transcriptional changes induced by WNT4 treatment (100 ng ml^{-1} WNT4 from day 26 to day 33) in wHILOs. Error bars represent ± s.e.m. $^*P < 0.05$, $^{**}P < 0.01$, $^{***}P < 0.001$, one-tailed, Student's paired *t*-test. Data representative of 3 independent experiments (**b**–**h**, **i** lower panel, **k**) or experimental triplicates (**i** upper panel, **l**).

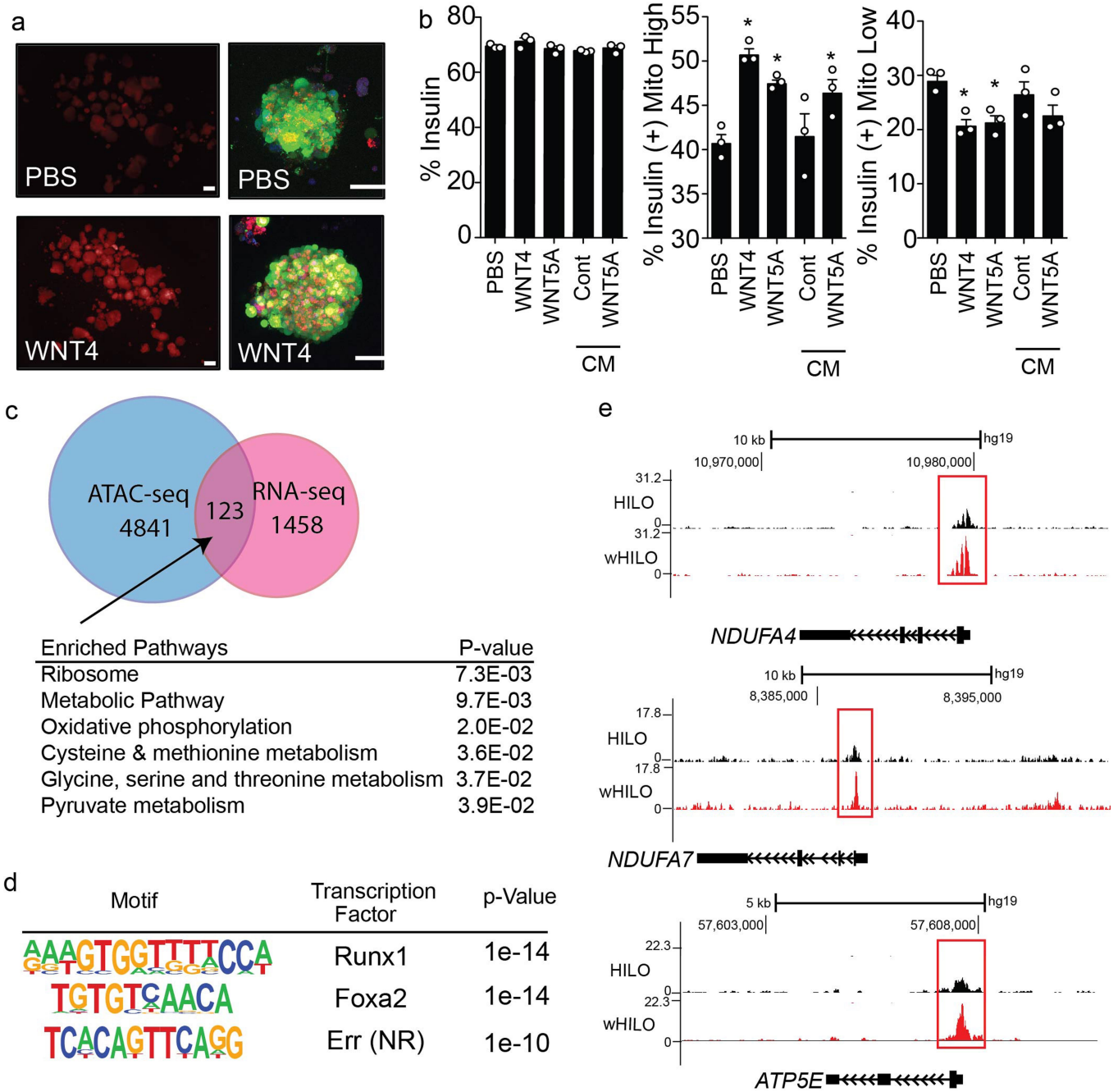

Extended Data Fig. 4 | WNT4 promotes mitochondrial maturation of HILOs. **a**, Representative images of insulin-GFP expression and MitoTracker staining (red) in PBS- and WNT4-treated HILOs (scale bar, 100 μm). **b**, Flow cytometry quantification of insulin expression (GFP) and mitochondrial content in HILOs treated with recombinant human WNT4 (rhWNT4), WNT5A (rhWNT5A), or conditioned media (CM) from control or WNT5A overexpressing fibroblasts ($n = 3$). **c**, Venn diagram showing overlap between WNT4-induced increases in chromatin accessibility in GFP$^+$ cells and increases in HILO gene expression (upper panel), and gene ontology pathways enriched in the intersection gene set. **d**, Motifs enriched in the intersection gene set from **c**. **e**, Chromatin accessibility at ERRγ target genes determined by ATAC–seq in insulin-expressing cells sorted from HILOs treated with PBS or WNT4 (wHILO) for 7 days (fold change >1.5). Error bars represent ± s.e.m. *$P < 0.05$, one-tailed, Student's paired t-test. Data representative of 3 (**a**, **b**) or 2 (**c**–**e**) independent experiments.

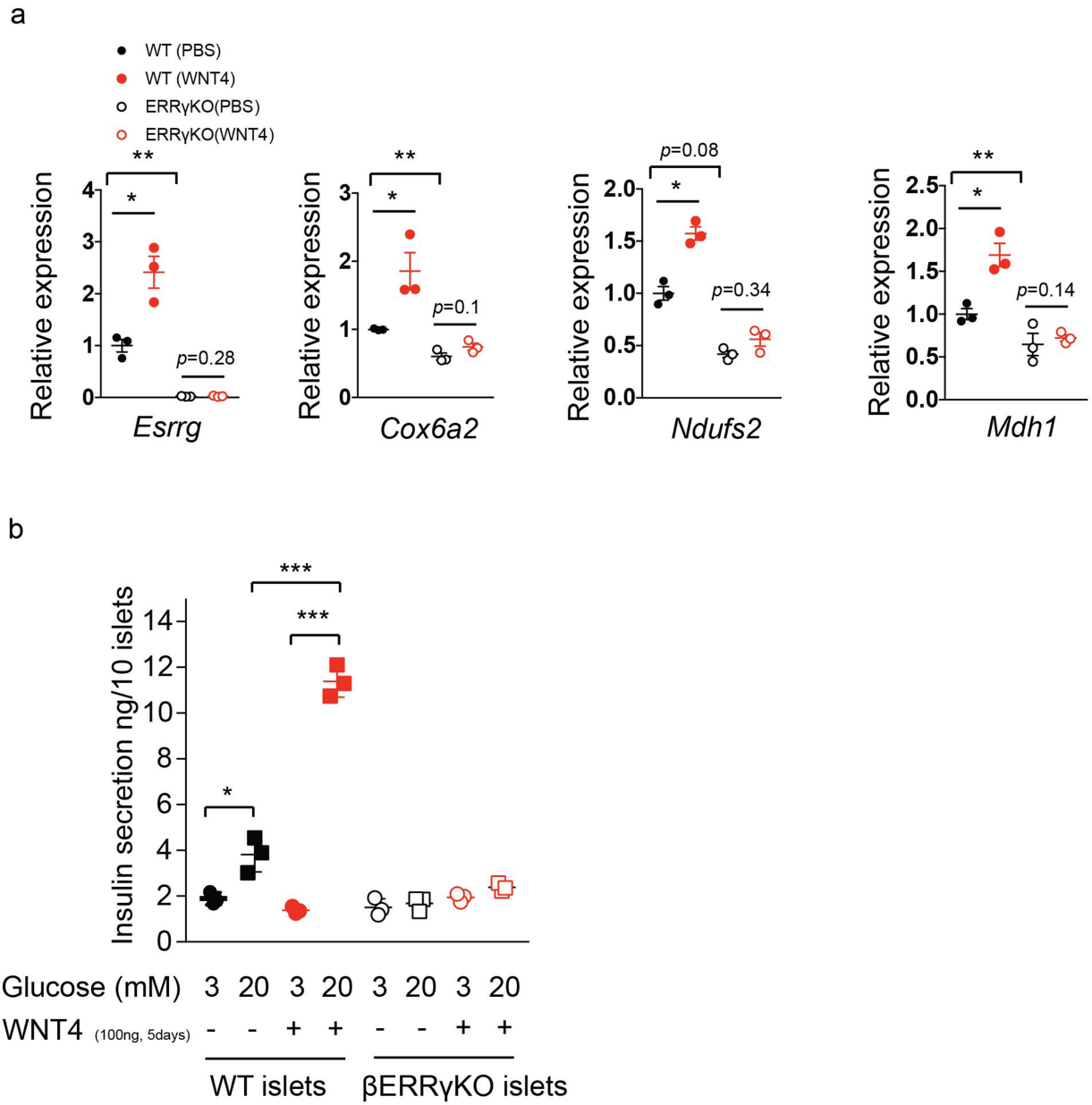

Extended Data Fig. 5 | ERRγ is required for WNT4-driven metabolic maturation. a, **b**, Postnatal islets (day P11-14) from WT and β cell specific ERRγKO mice were cultured with or without rhWNT4 (100 ng ml^{-1}) for >5 days. Relative gene expression measured by qPCR (**a**), and insulin secretion in response to 3 mM and 20 mM glucose (**b**). $n = 3$. Error bars represent ± s.e.m. $^{*}P < 0.05$, $^{**}P < 0.01$, $^{***}P < 0.001$, one-tailed, Student's paired t-test. Data representative of 2 independent experiments (**a**, **b**).

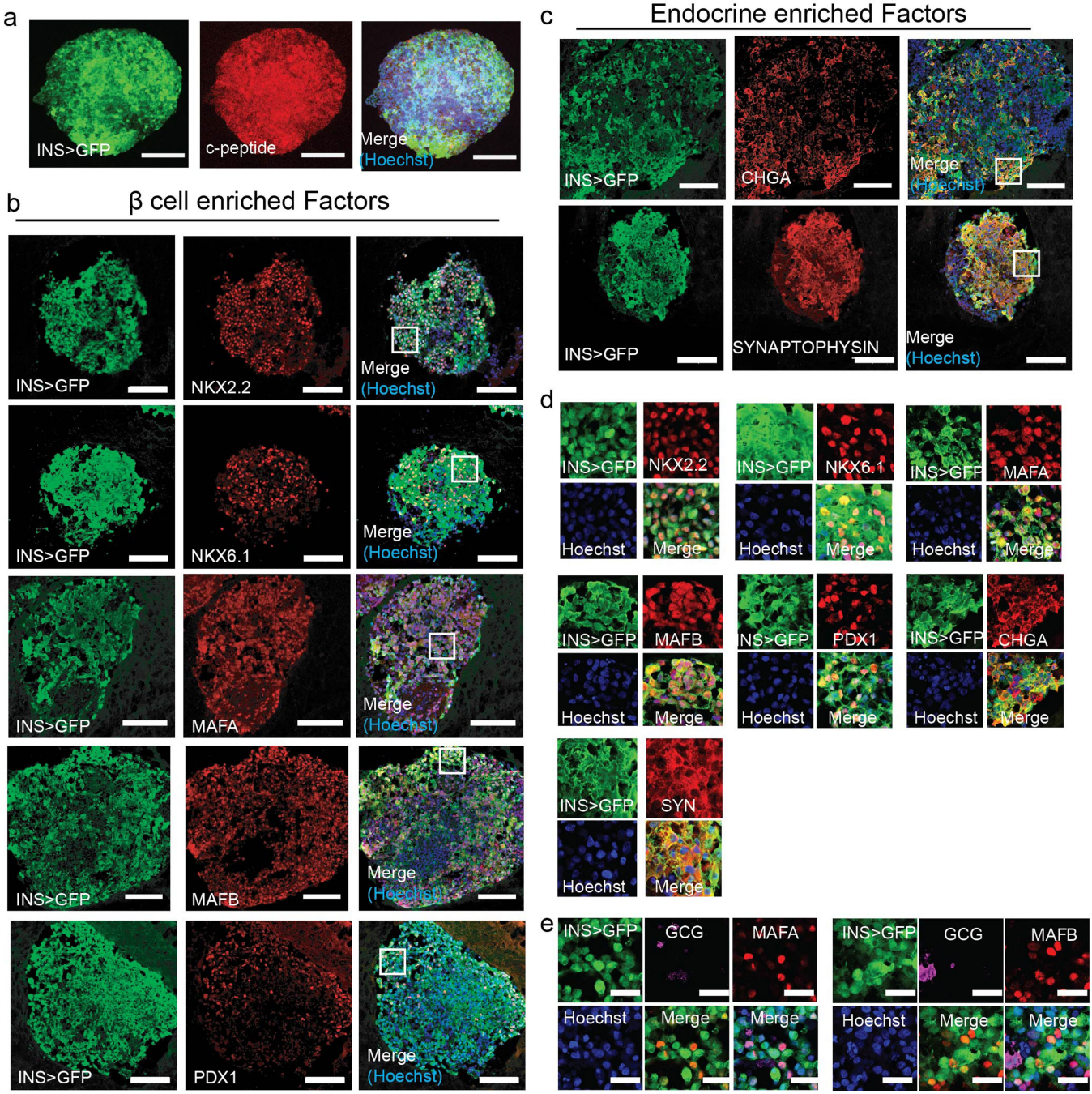

Extended Data Fig. 6 | Immunofluorescence characterization of wHILOs. **a**–**c**, Confocal images of wHILOs stained for C-peptide (**a**), β cell enriched markers NKX2-2, NKX6-1, MAFA, MAFB, PDX1 (**b**), and endocrine markers chromogranin A (CHGA), Synaptophysin (red) with Insulin-GFP (green) visualization (**c**). **d**, Magnification of 75 µm x 75 µm boxed regions shown in **b** and **c**. **e**, Immunofluorescence images of wHILOs showing insulin (GFP), β cell markers MAFA and MAFB, and α cell marker glucagon expression. Hoechst nuclei staining (blue). Scale bar: 100 µm (**a**–**c**), 10 µm (**e**). Images are representative of 3 independent experiments.

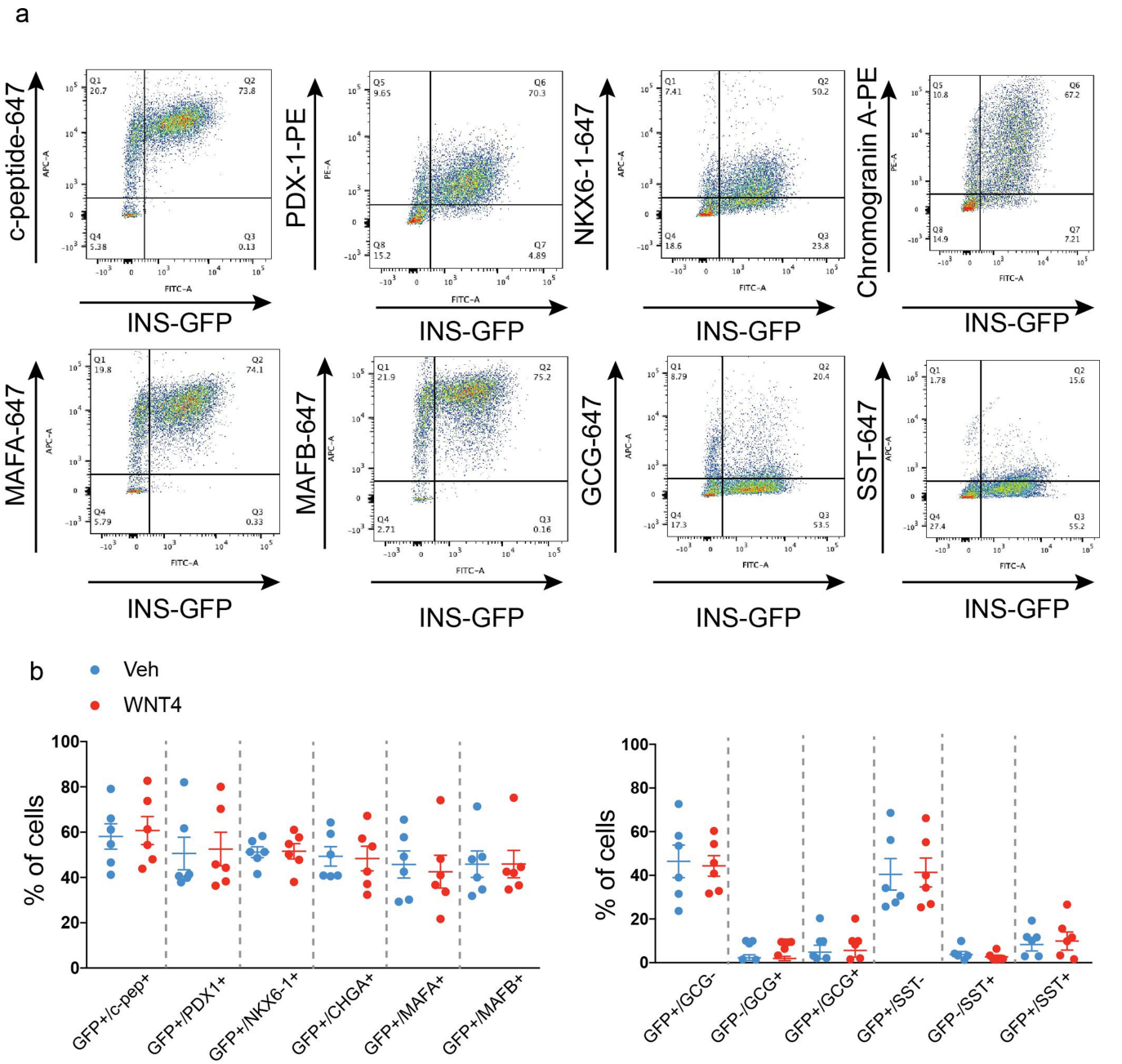

Extended Data Fig. 7 | Flow cytometry analysis of HILOs. a, Representative flow cytometry results for β cell and endocrine marker co-staining in HILOs with and without WNT4 treatment. **b**, Quantification of results in **a** ($n = 6$).

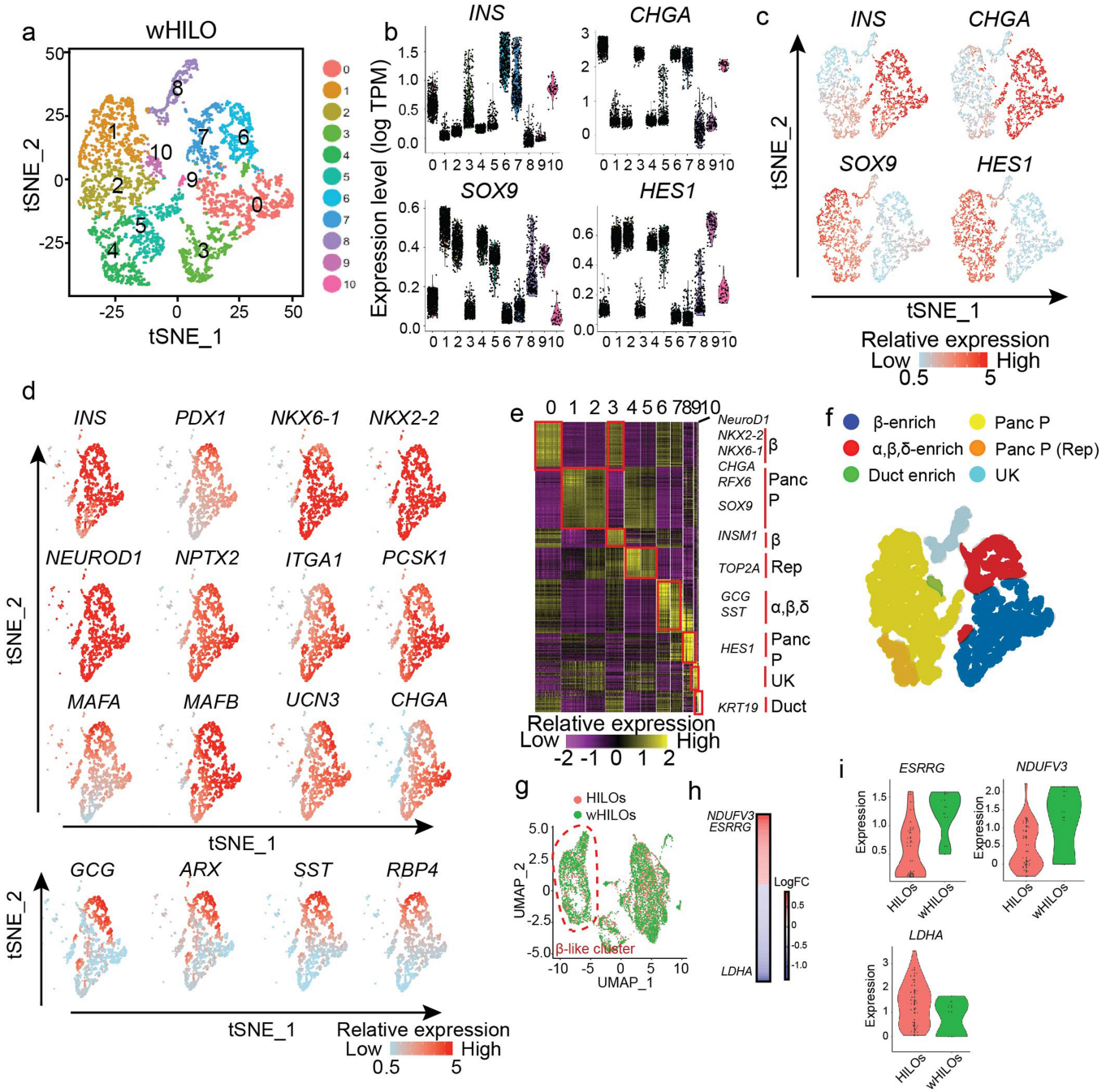

Extended Data Fig. 8 | Single cell analysis of wHILOs. a, *t*-SNE clustering of single cell transcriptomes from WNT4-treated HILOs (wHILOs, $n = 4840$). **b**, **c**, Violin plots (**b**) and single-cell expression (**c**) of *INS*, *CHGA*, *SOX9*, *HES1* in wHILOs. **d**, Expression of β cell-enriched (*INS*, *PDX1*, *NKX6-1*, *NKX2-2*, *NEUROD1*, *NPTX2*, *ITGA1*, *PCSK1*, *MAFA*, *MAFB*, *UCN3*, *CHGA*), α cell-enriched (*GCG*, *ARX*) and δ cell-enriched genes (*SST*, *RBP4*) overlaid on *t*-SNE clustering. **e**, Heat map of top 10 differentially expressed genes in each cell cluster. **f**, *t*-SNE clusters coloured according to cell type (Panc *P* = pancreatic progenitor, Rep = replicating, UK = unknown). **g**, UMAP clustering of combined HILOs and wHILO single cell datasets after expression restoration of sparse counts using SAVER. **h**, Heat map shows the differentially expressed genes (logFC) between HILOs and wHILOs in *ESRRG* and *INS* double positive cells using *WhichCells* function (expression >0.1). **i**, Distribution of *ERRγ* (*ESRRG;* min: 0.10, 0.50; 1st Q: 0.14, 1.15; mean: 0.54, 1.22; 3rdQ 0.90, 1.56; max: 1.60, 1.60 for HILOs and wHILOs respectively), *NDUFV3* (min: −0.31, 1.21; 1stQ; −0.01, 1.33; mean: 0.49, 1.67; 3rdQ 1.00, 1.98; max: 2.22, 2.14 for HILOs and wHILOs respectively), *LDHA* (min: 0.05, 1.02; 1stQ; 0.50, 1.21; mean: 1.35, 1.33; 3rdQ 1.90, 1.44; max: 3.53, 1.67 for HILOs and wHILOs respectively) gene expression in *ESRRG* and *INS* double-positive HILOs ($n = 38$) and wHILOs ($n = 9$). Data pooled from three independent samples (**a**–**i**).

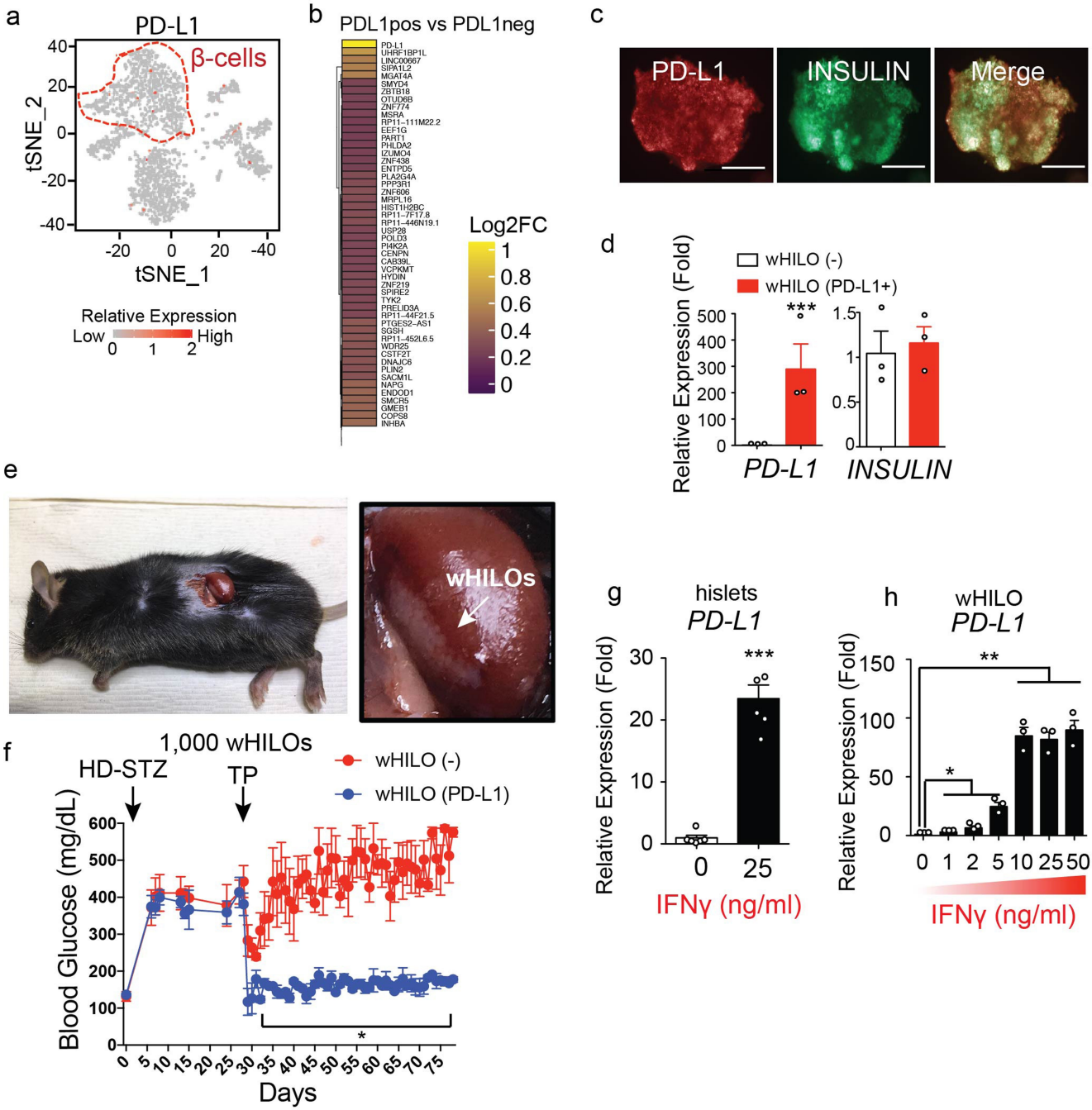

Extended Data Fig. 9 | PD-L1 expression in HILOs. a, Endogenous *PD-L1* expression highlighted in red in human islet cells ($n = 3,245$) (β cells are outlined in red). **b**, Heat map of top differentially expressed genes between PD-L1$^+$ and PD-L1$^-$ β cells. **c**, Immunohistochemistry showing overlap of lentiviral-driven PD-L1 expression and insulin promoter-driven GFP expression in wHILOs (scale bar, 100 µm). **d**, Human *PD-L1* and human insulin expression in wHILOs with and without lentiviral *PD-L1* overexpression, as measured by qPCR ($n = 3$). **e**, Transplantation of PD-L1 overexpressing wHILOs into the kidney capsule of STZ-induced diabetic mice. **f**, Blood glucose levels of C57BL6J mice treated with high dose streptozotocin (HD-STZ) before transplantation of wHILOs with and without PD-L1 overexpression (500 wHILOs into each kidney, total 1,000 wHILOs) ($n = 3$). **g**, *PD-L1* expression in human islet 12 h after IFN-γ stimulation ($n = 5$). **h**, *PD-L1* expression in wHILOs 12 h after indicated IFN-γ stimulation ($n = 3$). Error bars represent ± s.e.m. $^*P < 0.05$, $^{**}P < 0.01$, $^{***}P < 0.001$, one-tailed, Student's paired *t*-test. Data were pooled from 3 independent samples (**a**) or representative of 3 independent experiments (**c**, **d**, **g**, **h**).

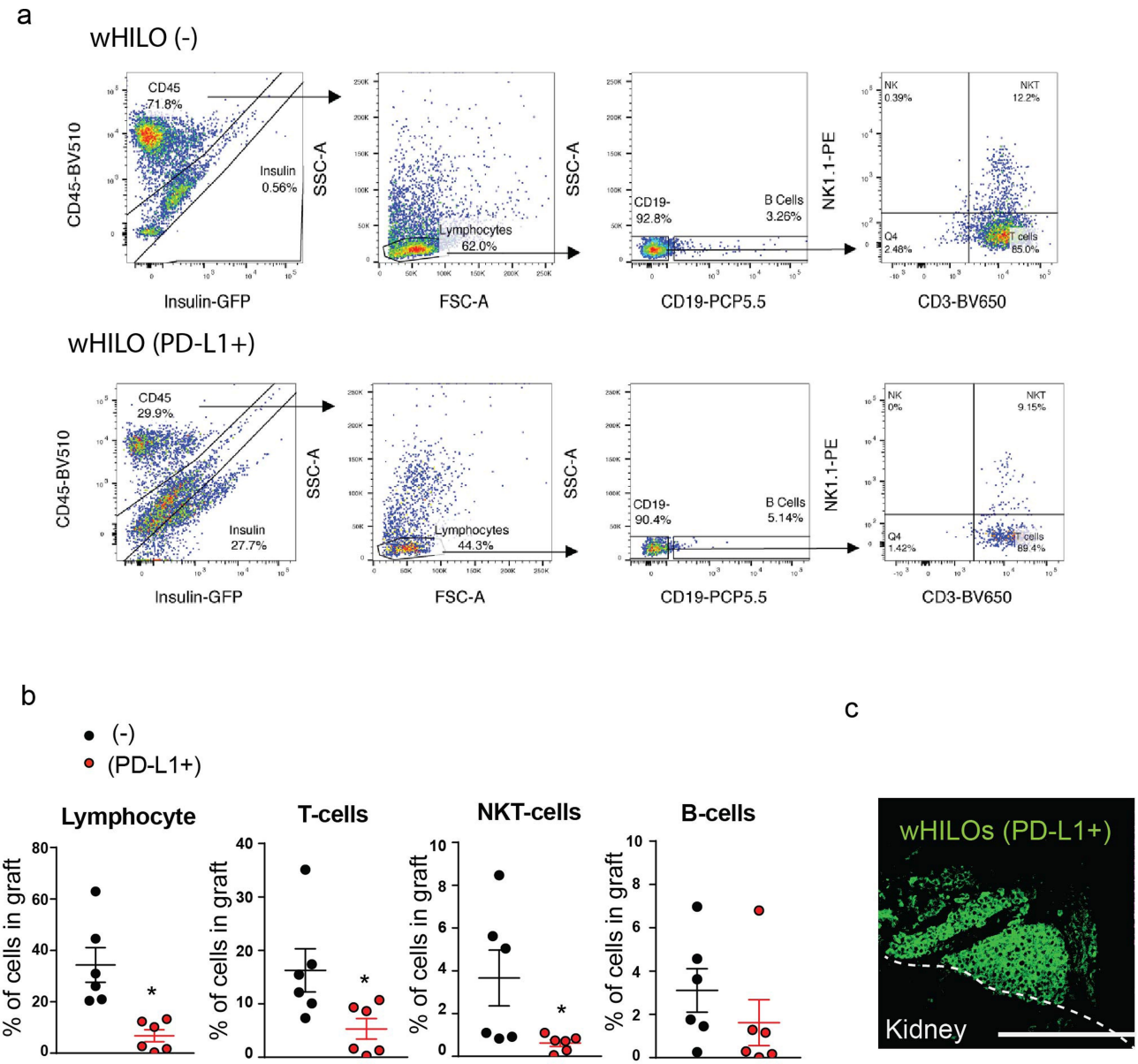

Extended Data Fig. 10 | Immune profiling of C57BL6J wHILO grafts. a, Flow cytometry analysis of insulin expressing and mouse immune (CD45$^+$) cells recovered from kidney capsule grafts 27 days after transplantation of wHILOs with and without PD-L1 expression. CD45$^+$ cells were further categorized as B cells (CD19$^+$), T cells (CD3$^+$) and NK cells (NK1.1$^+$). **b**, Quantification of **a**, ($n = 6$ and 6). **c**, wHILO (PD-L1) cells in kidney graft 27 days after transplantation (insulin promoter driven GFP expression). Scale bar, 100 µm. Error bars represent ± s.e.m. *$P < 0.05$, one tailed, Student's paired t-test. Data representative of 2 independent experiments.

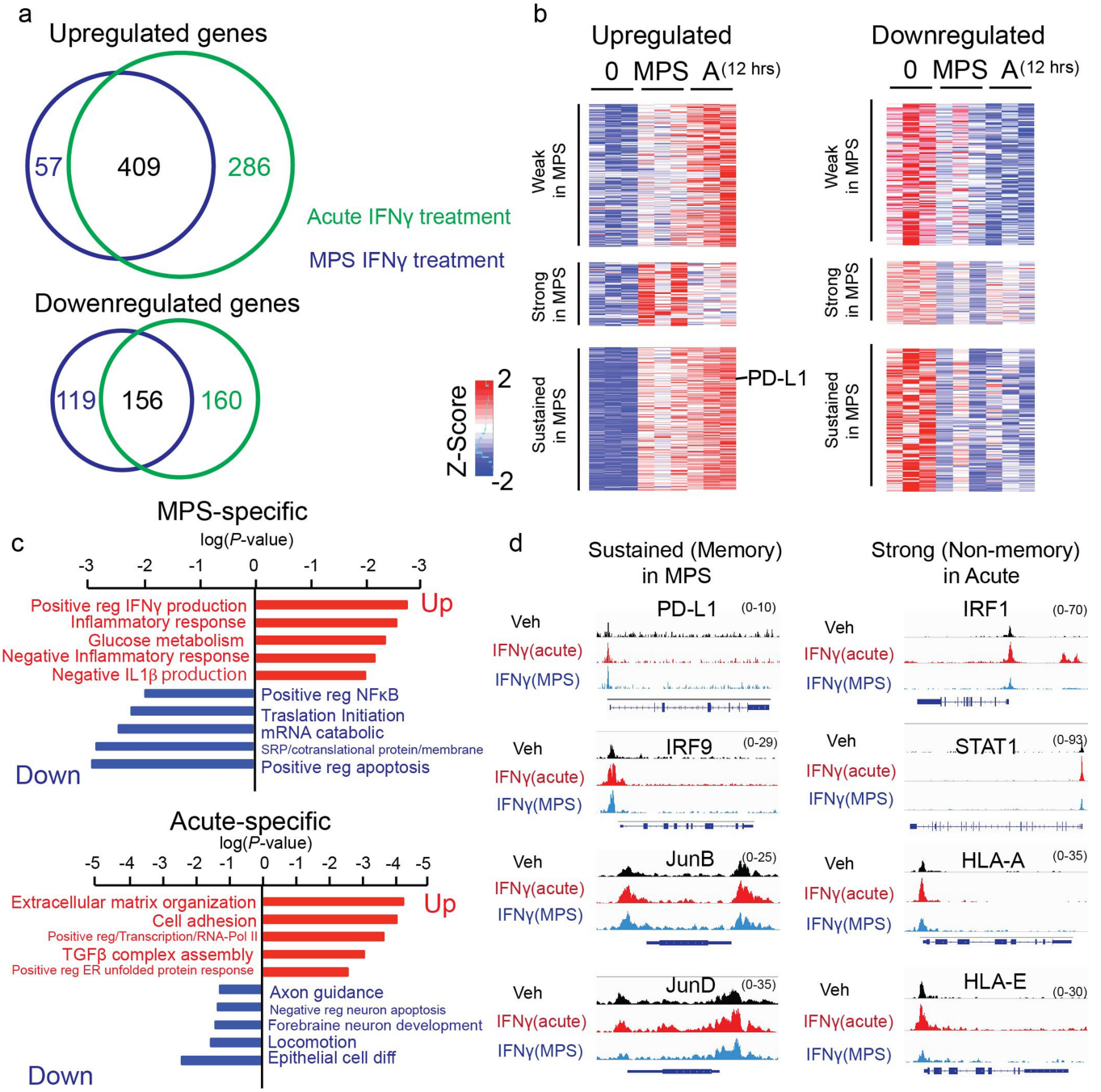

Extended Data Fig. 11 | IFN-γ-induced changes in wHILOs. a, Venn diagram of differentially regulated genes upon acute (12 h at 10 ng ml^{-1}) and multi pulse-stimulated (MPS; 2 h at 10 ng ml^{-1} for 3 days) IFN-γ treatment of wHILOs. **b**, Heat map of differentially expressed genes upon acute and MPS IFN-γ stimulation. Sustainable PD-L1 gene expression by MPS is indicated. **c**, Gene ontology of selectively regulated genes upon MPS-IFN-γ (top panel) and acute IFN-γ (bottom panel) treatments. **d**, Browser tracks showing chromatin accessibility at selected genes 7 days after last IFN-γ treatment in MPS or 12 h after acute IFN-γ stimulation in wHILOs. Data were from triplicate (**a**–**c**) or duplicate (**d**) samples.

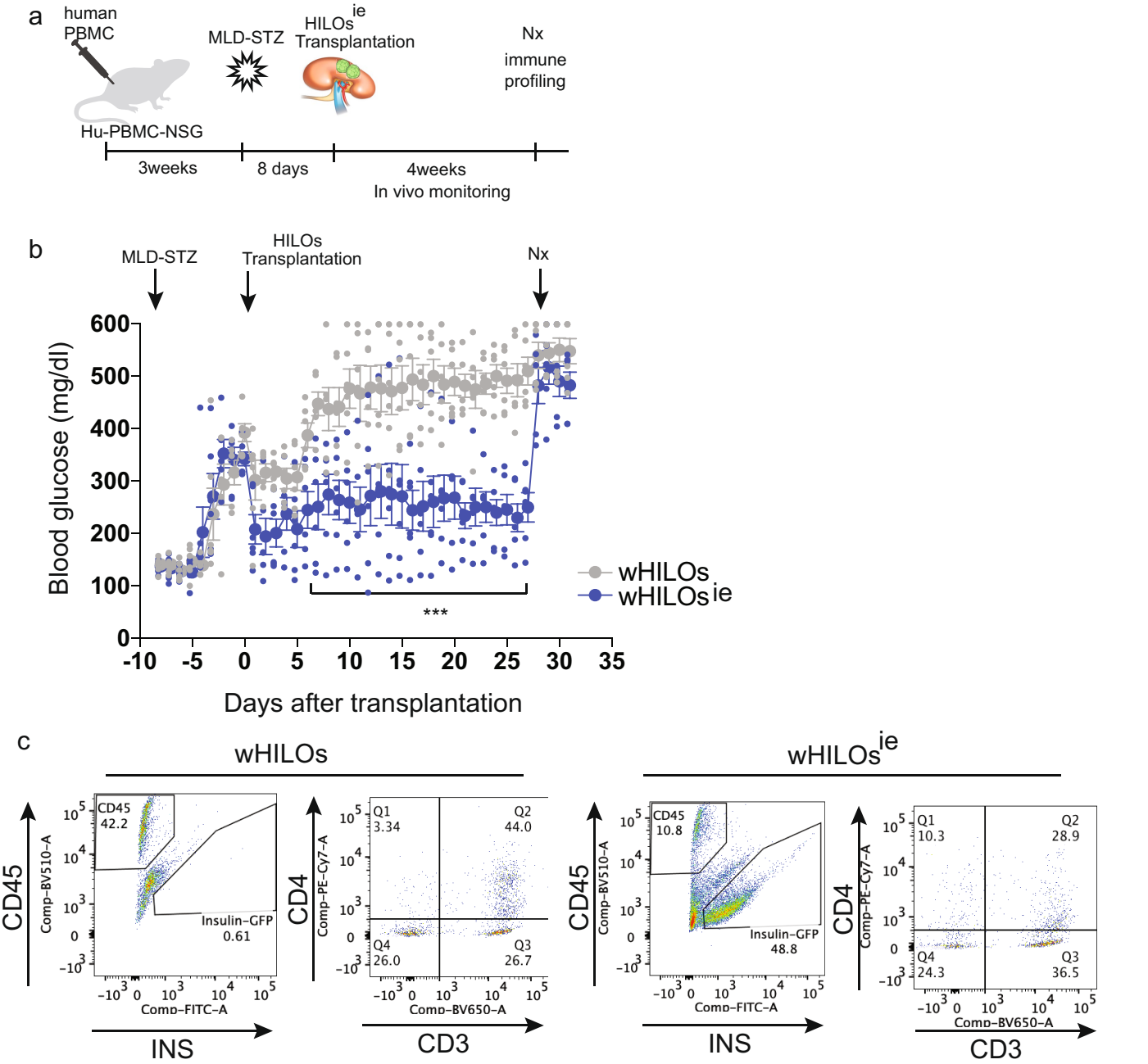

Extended Data Fig. 12 | Immune evasive wHILOs by enhanced endogenous PD-L1 expression. a, Schematic showing multi-low dose streptozotocin treatment (MLD-STZ, 50 mg/kg/day for 5 days) of Hu-PBMC-NSG mice to make immune competent diabetic model. MPS induced PD-L1 expressing wHILOs ($n = 500$) were transplanted under kidney capsule. **b**, Random-fed blood glucose levels in STZ-induced diabetic Hu-PBMC-NSG mice after transplantation of wHILOs with or without MPS ($n = 6$). Data for wHILOs (−) from Fig. 3c was used since those experiments were performed in parallel. **c**, Flow cytometry analyses of insulin-expressing and human immune ($CD45^+$) cells recovered from kidney capsule grafts 27 days after transplantation of wHILOs with or without MPS. Error bars represent ± s.e.m. $^*P < 0.05$, $^{**}P < 0.01$, $^{***}P < 0.001$, one-tailed, Student's paired t-test. Data were compiled from **b** or representative of 2 independent experiments.

nature research

Corresponding author(s): Ronald M Evans

Last updated by author(s): 4/31/20

Reporting Summary

Nature Research wishes to improve the reproducibility of the work that we publish. This form provides structure for consistency and transparency in reporting. For further information on Nature Research policies, see Authors & Referees and the Editorial Policy Checklist.

Statistics

For all statistical analyses, confirm that the following items are present in the figure legend, table legend, main text, or Methods section.

n/a	Confirmed	
☐	☒	The exact sample size (*n*) for each experimental group/condition, given as a discrete number and unit of measurement
☐	☒	A statement on whether measurements were taken from distinct samples or whether the same sample was measured repeatedly
☐	☒	The statistical test(s) used AND whether they are one- or two-sided *Only common tests should be described solely by name; describe more complex techniques in the Methods section.*
☐	☒	A description of all covariates tested
☐	☒	A description of any assumptions or corrections, such as tests of normality and adjustment for multiple comparisons
☐	☒	A full description of the statistical parameters including central tendency (e.g. means) or other basic estimates (e.g. regression coefficient) AND variation (e.g. standard deviation) or associated estimates of uncertainty (e.g. confidence intervals)
☐	☒	For null hypothesis testing, the test statistic (e.g. *F*, *t*, *r*) with confidence intervals, effect sizes, degrees of freedom and *P* value noted *Give P values as exact values whenever suitable.*
☒	☐	For Bayesian analysis, information on the choice of priors and Markov chain Monte Carlo settings
☐	☒	For hierarchical and complex designs, identification of the appropriate level for tests and full reporting of outcomes
☐	☒	Estimates of effect sizes (e.g. Cohen's *d*, Pearson's *r*), indicating how they were calculated

Our web collection on statistics for biologists contains articles on many of the points above.

Software and code

Policy information about availability of computer code

Data collection	FACS Aria, FACS Canto II, LSR II were used to collect FACS Data. Zeiss LSM 880 Rear Port Laser Scanning Confocal and Airyscan FAST Microscope were used for imaging. All open resource and software used for the study were described in the manuscript. Software or program listed below were used for genomic data analysis 1. R studio (https://www.rstudio.com/) 2. Cell Ranger R Kit (https://support.10xgenomics.com/single-cell-gene-expression/software/pipelines/latest/rkit) ver 2.0.2 3. Seurat (https://satijalab.org/seurat/) ver 2.0 4. DAVID (https://david.ncifcrf.gov/home.jsp) 5. GOplot (https://wencke.github.io) 6. UCSC genome browser (http://genome.ucsc.edu) 7. Homer (http://homer.ucsd.edu/homer/)
Data analysis	All open resource, software and methods for analysis used for the study were described in the material and methods section of this manuscript. Graph data were analysed by Graphpad Prism 7 or Microsoft Excel. Software or program listed below were used for genomic data analysis 1. R studio (https://www.rstudio.com/) 2. Cell Ranger R Kit (https://support.10xgenomics.com/single-cell-gene-expression/software/pipelines/latest/rkit) ver 2.0.2 3. Seurat (https://satijalab.org/seurat/) ver 2.0 4. DAVID (https://david.ncifcrf.gov/home.jsp) 5. GOplot (https://wencke.github.io) 6. UCSC genome browser (http://genome.ucsc.edu) 7. Homer (http://homer.ucsd.edu/homer/)

For manuscripts utilizing custom algorithms or software that are central to the research but not yet described in published literature, software must be made available to editors/reviewers. We strongly encourage code deposition in a community repository (e.g. GitHub). See the Nature Research guidelines for submitting code & software for further information.

Data

Policy information about availability of data

All manuscripts must include a data availability statement. This statement should provide the following information, where applicable:

- Accession codes, unique identifiers, or web links for publicly available datasets
- A list of figures that have associated raw data
- A description of any restrictions on data availability

RNA-Seq and ATAC-Seq data reported in this paper have been deposited in the National Center for Biotechnology Information (NCBI) Sequence Read Archive (SRA) database, Accession # PRJNA505532.
- Fig. 1a-d; 2d,h,i; 3b
-Ext.Data Fig. 1a,i; 2a,b; 3j; 4c-e; 8a-i; 9a,b; 11a-d
-No restriction for data availability.

Source Data provided for all graph figures

Field-specific reporting

Please select the one below that is the best fit for your research. If you are not sure, read the appropriate sections before making your selection.

☒ Life sciences ☐ Behavioural & social sciences ☐ Ecological, evolutionary & environmental sciences

For a reference copy of the document with all sections, see nature.com/documents/nr-reporting-summary-flat.pdf

Life sciences study design

All studies must disclose on these points even when the disclosure is negative.

Sample size	Sample size were determined empirically based on preliminary experimental findings. For transplantation experiments in C57BL6J and NOD-SCID mice, preliminary experiments were performed with a minimum of 2 mice, and full cohort experiments repeated at least twice. The transplantation experiments in HuPBMC-NSG mice were repeated in more than 2 independent experiments. Experiment in Extended Data Fig.9f was performed once. HILOs generation has been repeated >50 times.
Data exclusions	On principle, data were only excluded for failed experiments. Failed experiments were determined by positive and negative control experiments.
Replication	Replicate experiments were successful. Every experiment was performed multiple times with essentially the same results
Randomization	Sex-matched littermates were randomly assigned to experimental arms. STZ treated mice were grouped based on serum glucose levels, and mice with the highest levels utilized for positive control experiments (i.e. mouse and human islet transplantations in Figures 3d and Extended 1g). Prior to transplantation, HILOs functionality was confirmed based on Insulin, MafA, UCN3, Esrrg and PD-L1 expression, determined by qpcr.
Blinding	No blinding was performed.

Reporting for specific materials, systems and methods

We require information from authors about some types of materials, experimental systems and methods used in many studies. Here, indicate whether each material, system or method listed is relevant to your study. If you are not sure if a list item applies to your research, read the appropriate section before selecting a response.

Materials & experimental systems

n/a	Involved in the study
☐	☒ Antibodies
☐	☒ Eukaryotic cell lines
☒	☐ Palaeontology
☐	☒ Animals and other organisms
☒	☐ Human research participants
☒	☐ Clinical data

Methods

n/a	Involved in the study
☒	☐ ChIP-seq
☐	☒ Flow cytometry
☒	☐ MRI-based neuroimaging

Antibodies

Antibodies used	The following antibodies were validated by previous publications as well as in our laboratory using IHC on human islets, mouse

islets and HILOs. All antibodies were used at a 1/100 dilution.

Validation

Antibody	supplier	Cat #
Insulin	abcam	ab7842
c-peptide	abcam	ab30477
glucagon	abcam	ab10988
somatostatin	abcam	ab103790
PD-L1	abcam	ab20592
PDX-1	R&D Systems	AF2419
CHGA	abcam	ab15160
SYNAPTOPHYSIN	Biogenex	MU363-UC
NKX6-1	DSHB	F55A12
Pancreatic Polypeptide	abcam	ab113694
MAFA	abcam	ab26405 (Also confirmed MAFA Novus NB400-1377)
MAFB	abcam	ab66506 (Also confirmed MAFA Bethyl LAb A700-046)

For signal amplification (for MAFA and MAFB) the goat anti-rabbit poly-HRP secondary antibody was used (comes already premixed in goat serum, B40962, Thermo) and developed with TSA-Cy3 reagent (SAT704A001EA, Akoya Biosciences) for 10min. All antibodies were used at a 1/100 dilution and validated by staining human primary islets.

Eukaryotic cell lines

Policy information about cell lines

Cell line source(s)	human induced pluripotent stem cells derived from HUVECs (Salk Stem Cell Core). HuES8 (Harvard University). H1ES (Wicells). hiPSC derived Beta like cells (TAKARA, ChiPSC12&ChiPSC22). HEK293LTV (Cell Biolabs).
Authentication	hiPSC derived Beta like cells from TAKARA are authentificated by TAKARA. HEK293LTV cells are authentificated by Cell Biolabs.
Mycoplasma contamination	The absence of mycoplasma contamination was routinely confirmed at ~2 month intervals.
Commonly misidentified lines (See ICLAC register)	No commonly misidentified cell lines were used.

Animals and other organisms

Policy information about studies involving animals; ARRIVE guidelines recommended for reporting animal research

Laboratory animals	Age- (8 - 20 weeks) and background-matched male C57BL/6J (Stock No 000664), NOD-SCID mice (NOD.Cg-Prkdcscid Il2rgtm1Wjl/SzJ, Stock No 005557), β cell-specific ERRγ knockout mice, hu-PBMC-SGM3 mice (Called as humanized mice. Female NSG™ mice were injected with human peripheral blood mononuclear cells in NSG-SGM3 (Jackson 013062) strain)
Wild animals	The study did not involve wild animals.
Field-collected samples	The study did not involve samples collected from the field.
Ethics oversight	All animal studies were reviewed by Salk IACUC for approval. Human islets studies were reviewed by IIDP for approval.

Note that full information on the approval of the study protocol must also be provided in the manuscript.

Flow Cytometry

Plots

Confirm that:

☒ The axis labels state the marker and fluorochrome used (e.g. CD4-FITC).

☒ The axis scales are clearly visible. Include numbers along axes only for bottom left plot of group (a 'group' is an analysis of identical markers).

☒ All plots are contour plots with outliers or pseudocolor plots.

☒ A numerical value for number of cells or percentage (with statistics) is provided.

Methodology

Sample preparation	Sample preparation is described in Methods.
Instrument	FACS Aria, FACS Canto, LSR II
Software	FACS Diva for collection and FlowJo for analysis

Cell population abundance	Purity was assessed by staining for CD45 and GFP expression
Gating strategy	Relevant gating strategies are shown in Methods

☒ Tick this box to confirm that a figure exemplifying the gating strategy is provided in the Supplementary Information.